NASA/CR—97-206308

Advanced Low-Noise Research Fan Stage Design

Robert Neubert, Larry Bock, Eric Malmborg, and William Owen-Peer
United Technologies Corporation, Pratt & Whitney, East Hartford, Connecticut

Prepared under Contract NAS3–26618

National Aeronautics and
Space Administration

Lewis Research Center

December 1997

Available from

NASA Center for Aerospace Information
800 Elkridge Landing Road
Linthicum Heights, MD 21090-2934
Price Code: A04

National Technical Information Service
5287 Port Royal Road
Springfield, VA 22100
Price Code: A04

FOREWORD

This report presents the results of the design of an Advanced Low-Noise Research Fan Stage. This design incorporates many advanced technology features to improve specific fuel consumption and reduce noise. The fan stage will be integrated into a powered subscale nacelle model for combined aerodynamic, acoustic, and structural testing of these features.

This design was conducted as Task XLIX under the Large Engine Technology (LET) program, National Aeronautics and Space Administration (NASA) Contract NAS3-26618, under the direction of Dennis Huff, NASA Project Manager.

The NASA task manager for Task XLIX was Brian Fite, NASA Lewis Research Center (LeRC), and Robert Neubert was task manager for Pratt & Whitney (P&W). Acknowledgments are given to the following P&W principal contributors for their efforts in the following areas:

Fan Aerodynamics	Robert Neubert, David Spear, William Sprout, David Hopwood
Acoustics	Lawrence Bock, John Low, Douglas Mathews
Structures	Eric Malmborg, William Owen-Peer
Mechanical Design	Gregory Reinhardt
Belcan	Jay Benson, Kevin Bowers, Pat Callahan, Scott Brown.

The continued interest and active participation of NASA LeRC personnel and their respective counterparts in the design of this fan stage was a significant benefit to the design process.

SUMMARY

This report describes the design of the Advanced Low-Noise Research Fan stage. The fan is a variable pitch design, which is designed at the cruise pitch condition. Relative to the cruise setting, the blade is closed at takeoff and opened for reverse thrust operation. The fan stage is a split flow design with fan exit guide vanes (FEGVs) and core stators.

The fan stage design is combined with a nacelle and engine core duct to form a powered fan/nacelle subscale model. This model is intended for use in combined aerodynamic, acoustic, and structural testing in a wind tunnel. The fan has an outer diameter of 22 in. and a hub-to-tip of 0.426 in., which allows the use of existing NASA fan and cowl force balance and rig drive systems. The design parameters were selected to permit valid acoustic and aerodynamic comparisons with the Pratt & Whitney (P&W) 17- and 22-in. rigs previously tested under NASA contract.

The fan stage design is described in detail. The results of the design axisymmetric and Navier-Stokes aerodynamic analysis are presented at the critical design conditions. The structural analysis of the fan rotor and attachment is included. The blade and attachment are predicted to have adequate low-cycle fatigue life and an acceptable operating range without resonant stress or flutter.

The stage was acoustically designed with airfoil counts in the FEGV and core stator to minimize noise. A fan/FEGV tone analysis developed separately under NASA contract was used to determine the optimum airfoil counts.

The fan stage was matched to the existing nacelle, designed under the previous P&W low-noise contract, to form a fan/nacelle model for wind tunnel testing. It is an axisymmetric nacelle for convenience in testing and analysis. Previous testing confirmed that the nacelle performed as required at various aircraft operating conditions.

CONTENTS

FIGURES

TABLES

1. INTRODUCTION

Major airports in the nation's air transportation system face a serious problem in providing greater capacity to meet the ever increasing demands of air travel. This problem could be relieved if airports are allowed to increase their operating time, now restricted by curfews and by relaxing present limits on takeoff and landings. A key operational issue in extending the present curfews is noise.

In response to these increasing restrictive noise regulations, NASA is executing a Noise Reduction Program as part of the Advanced Subsonic Technology Program. The goal of the program is to reduce the noise level of aircraft by a cumulative 30 dB, relative to 1992 technology, by the end of the decade. This implies noise reduction of 10 dB in each of the three aircraft flight phases where aircraft noise is measured — takeoff, sideline, and approach. A series of 22-inch fan tests are being conducted to investigate noise reduction concepts. The Pratt & Whitney (P&W) Fan 1 model completed testing in December 1995 in the 9 × 15 ft wind tunnel at NASA Lewis Research Center (LeRC).

An advanced low-noise fan stage has been designed to further reduce noise from lower fan tip speed and Navier-Stokes optimized blading. This report describes the aerodynamic, acoustic, and structural design of this model.

2. FAN STAGE AERODYNAMIC DESIGN

2.1 OBJECTIVE

The low-noise fan stage was designed to model a reduced speed low-noise research fan for use in combined acoustic, aerodynamic, and nacelle testing. The goal of the low-noise fan stage is to contribute to reducing engine noise approximately 6 dB, relative to 1992 technology, at each of the three flight conditions where aircraft noise is measured — takeoff, sideline, and approach. This fan stage was designed to reduce takeoff rotor speed 10 percent relative to the current 22 in. fan designed under NASA Contract NAS3-26618 Tasks 2 and 31 (Figure 1) with the main design constraint being this fan must fit within the current flowpath (Figure 2).

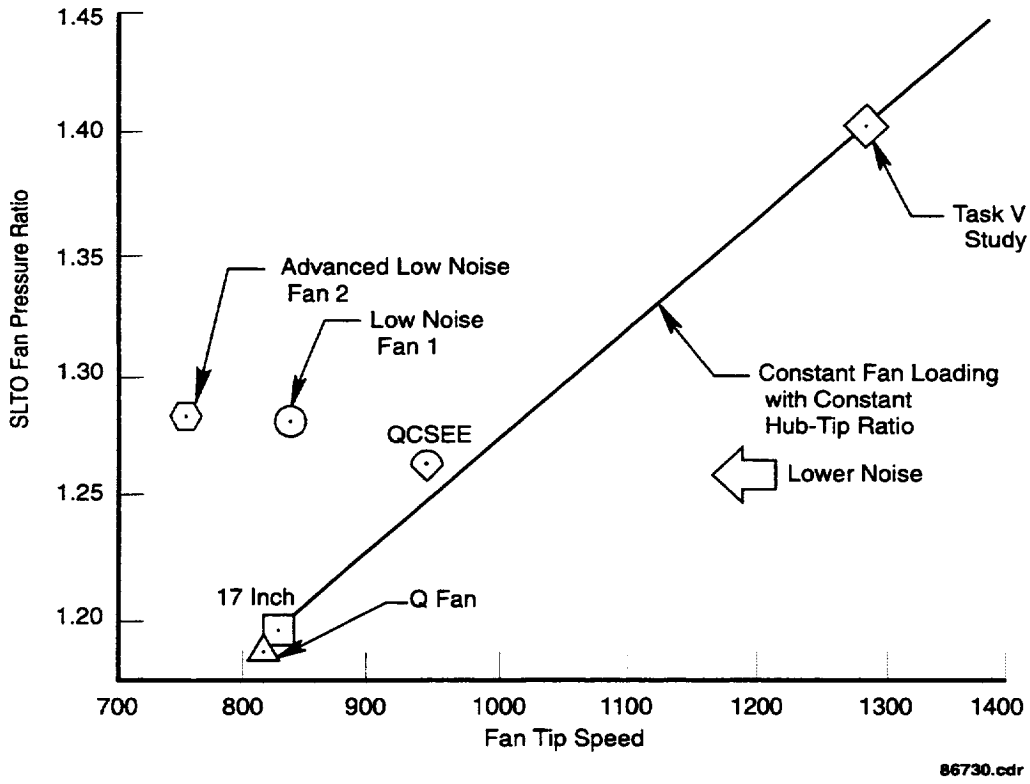

Figure 1. Low-Noise Fan Tip Speed Reduction

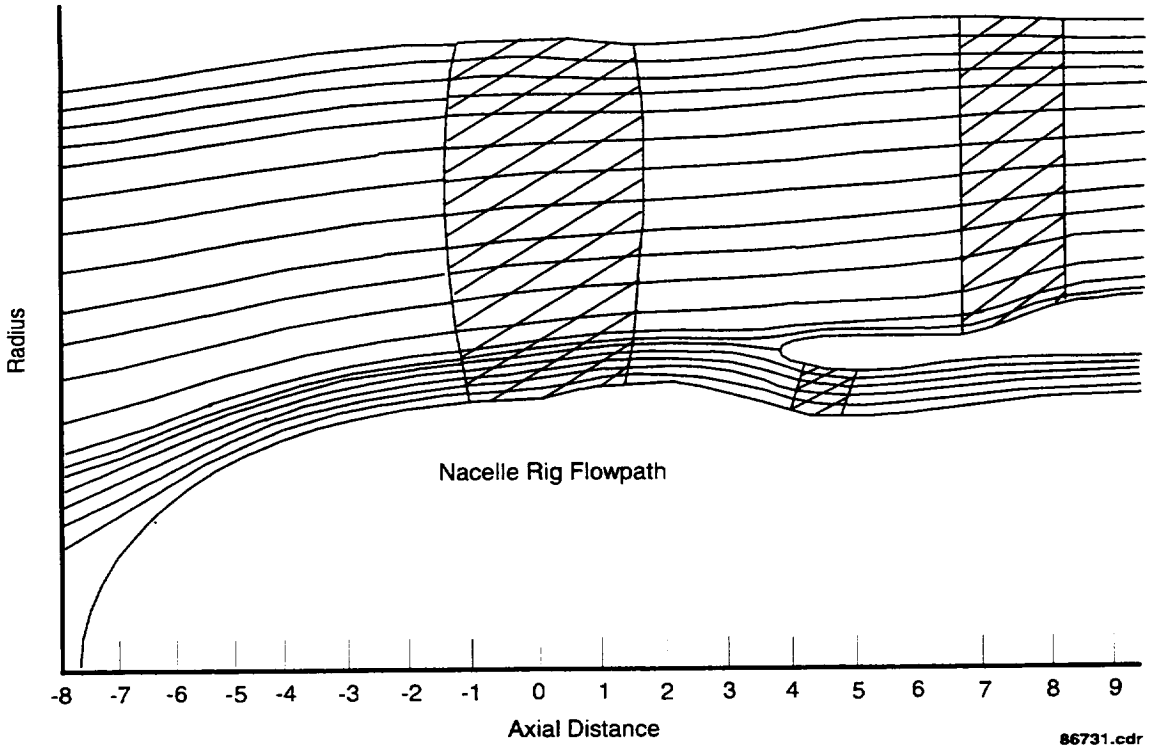

Figure 2. Low-Noise Rig Flowpath

2.2 FAN BLADE DESIGN

Table 1 compares the advanced low-noise fan design parameters to those of the current 22-in. low-noise fan and the 17-in. rig fan.

Table 1. Fan Design Parameters

Fan Parameters	*Fan/Nacelle 17 in. Rig*	*P&W-NASA Low-Noise Fan 1*	*P&W-NASA Advanced Low-Noise Fan 2*
Pressure Ratio (Duct, Stage)			
SLTO	1.20	1.284	1.284
Cruise	1.21	1.294	1.294
Approach	—	1.077	1.077
Cutback	—	1.209	1.209
Corrected rpm			
SLTO	11,675	8,750	7,875
Cruise	11,200	8,400	7,557
Approach	—	5,000	4,425
Cutback	—	7,740	6,950
Corrected U-tip (ft/sec)			
SLTO	836	840	756
Cruise	802	806	725
Approach	—	480	425
Cutback	—	743	667
Corrected W/A (lbm/sec ft^2)			
SLTO	32.6	36.9	36.9
Cruise	40.8	42.5	42.5
Approach	—	22.7	22.7
Cutback	—	33.3	33.3
Bypass Ratio — Cruise	20.4	13.3	13.3
Blade Number	16	18	18
Vane Number	22/40	45	51
Hub/Tip	0.443	0.426	0.426
Diameter — LE	17.0	22.0	22.0

See Appendix A for design velocity vectors and Appendix B for flowpath coordinates.

2.3 FAN BLADE OPTIMIZATION

Navier-Stokes three-dimensional (3-D) analysis of the Advanced Low-Noise Fan 2 indicated that boundary layer separation on the suction surface of the fan increased significantly, relative to baseline Low-Noise Fan 1 at takeoff (Figure 3), due to the lower fan speed increasing loading levels. To minimize this effect, radial work distribution and incidence were optimized (Figures 4 and 5). A small improvement was achieved with the outside diameter (OD) biased radial profile (Figure 6). Predicted fan wakes, although slightly larger than Low-Noise Fan 1, are not thought to be big enough to offset the acoustic benefit of lower tip speed (Figure 7).

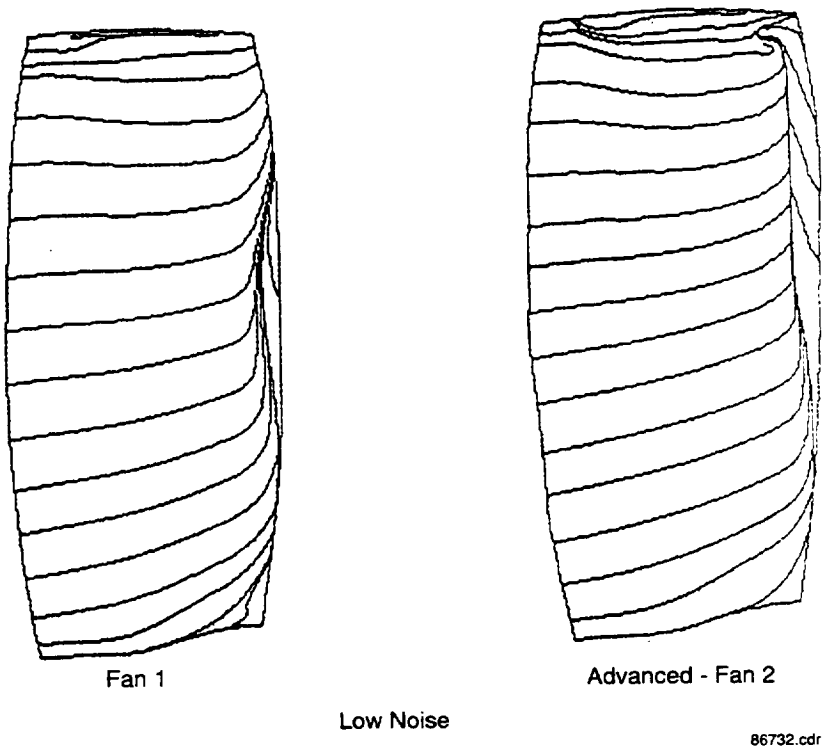

Figure 3. Fan Suction Surface Streakline Comparison at Takeoff

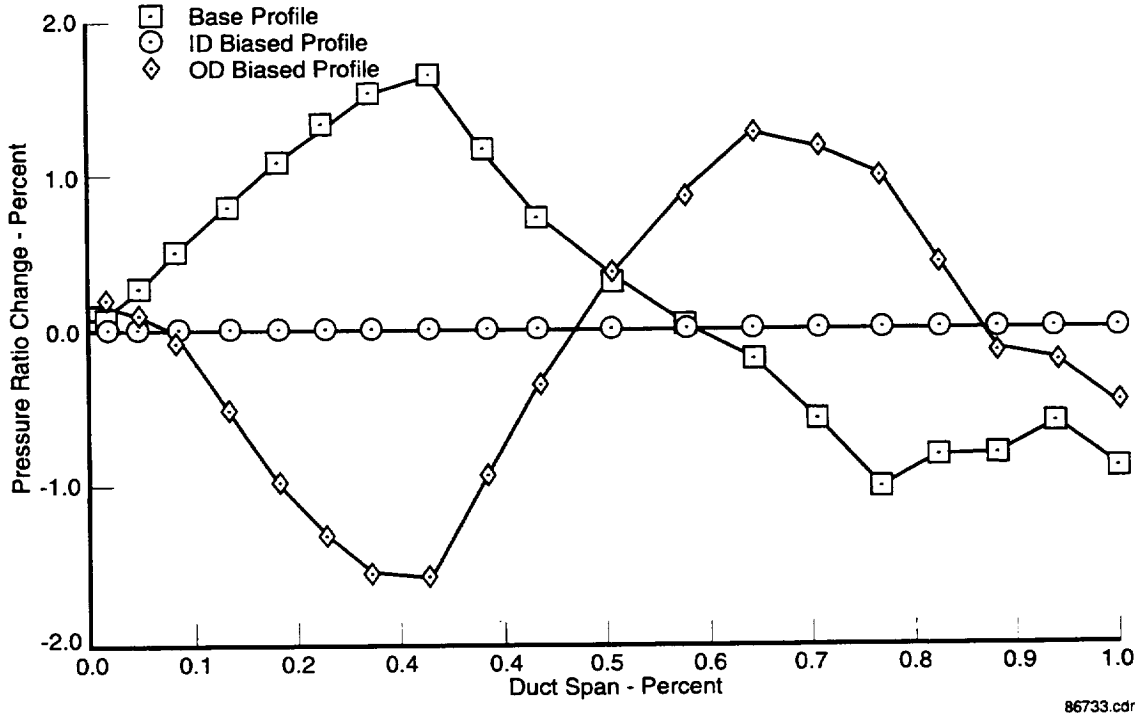

Figure 4. Fan Radial Work Optimization

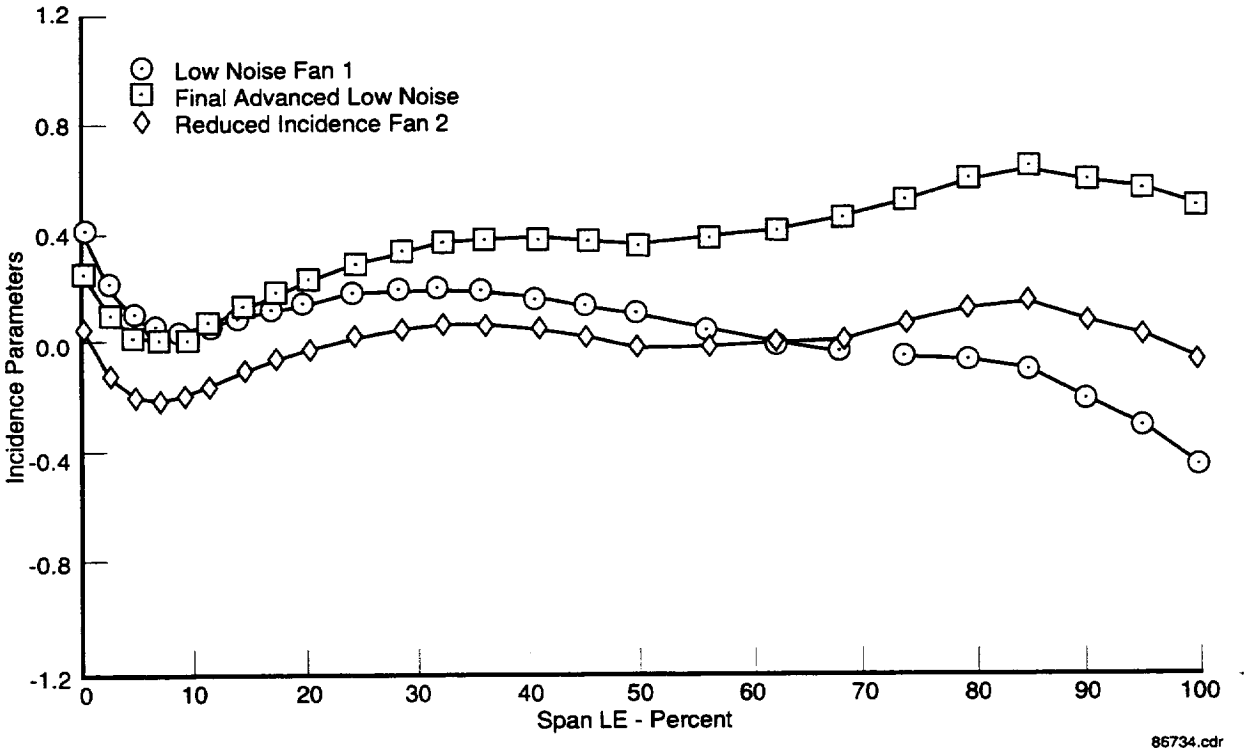

Figure 5. Low-Noise Fan Radial Incidence Optimization at Takeoff

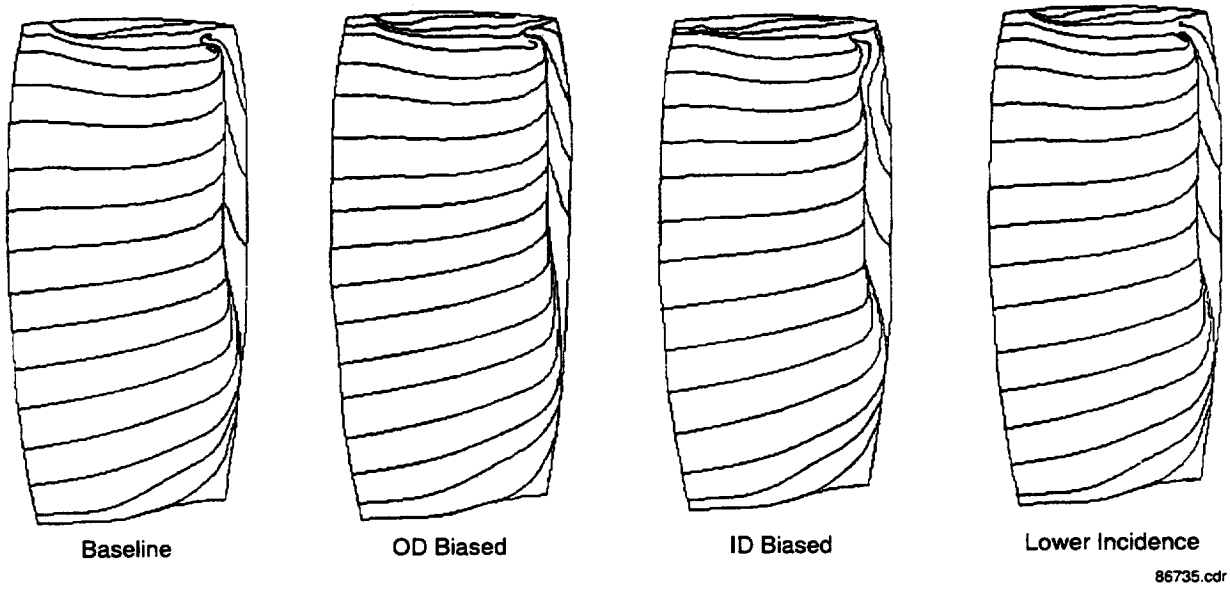

Figure 6. Fan Separation Reduction at Takeoff

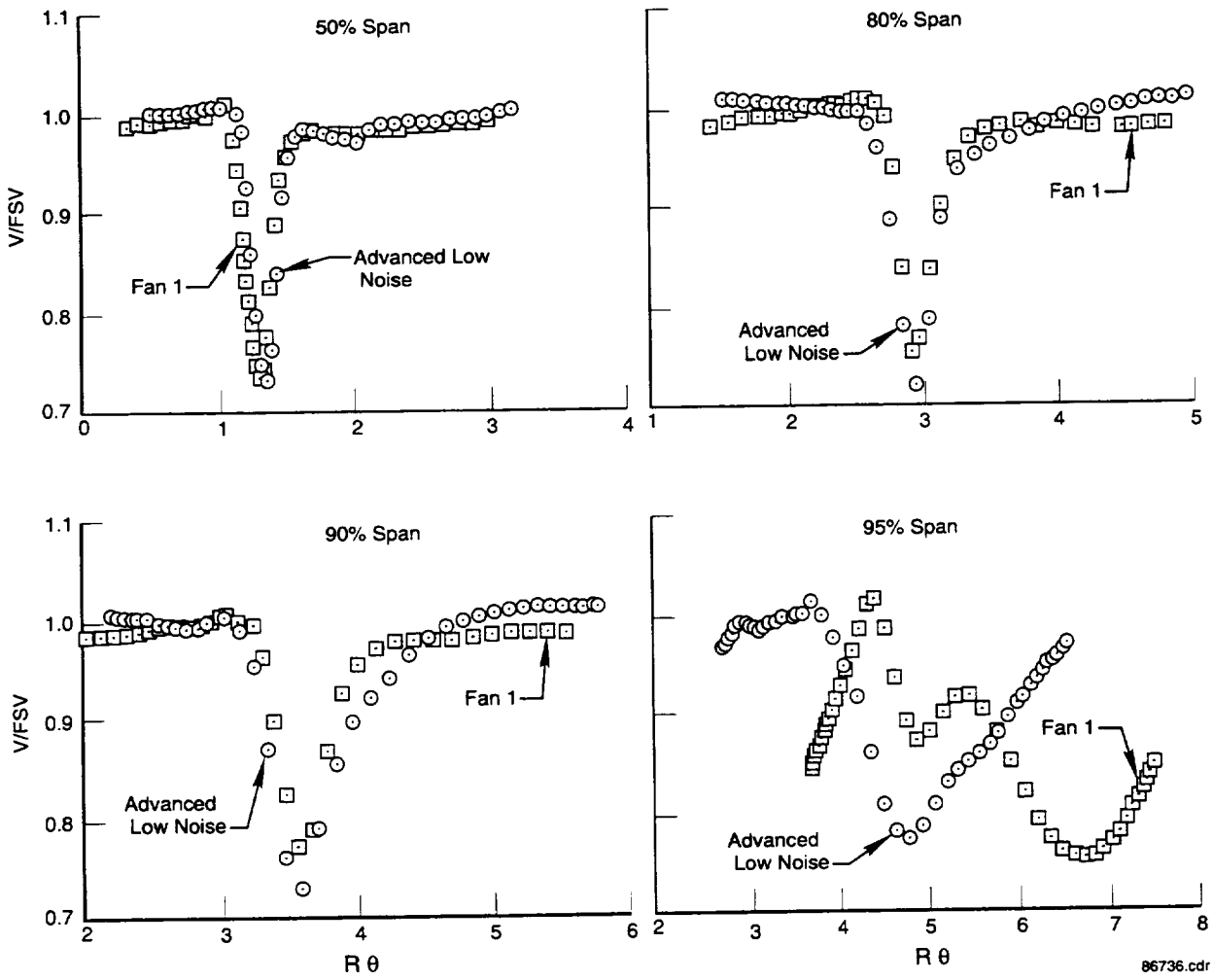

Figure 7. Fan Wake Comparisons

2.4 FAN BLADE AIRFOIL SECTIONS

Controlled diffusion airfoil sections were used for the fan rotor, similar to those used for Low-Noise Fan 1. Airfoil section parameters were optimized for good performance as shown in Figure 8.

At cruise and takeoff operating line conditions, all airfoil sections were predicted to be free of boundary layer separation at all spans, on a two-dimensional (2-D) basis. In addition, all sections were predicted to be separation-free at the maximum flow condition, indicating they could meet 2-D incidence and loading requirements (Figure 9). However, 3-D Navier-Stokes analysis did indicate that there would be some separation at the takeoff condition, as described previously in Section 2.3.

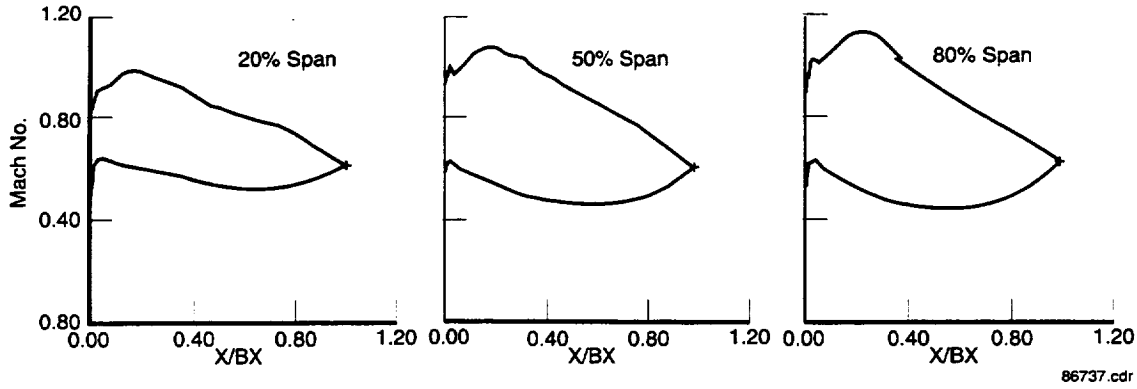

Figure 8. Fan Design Mach Distributions

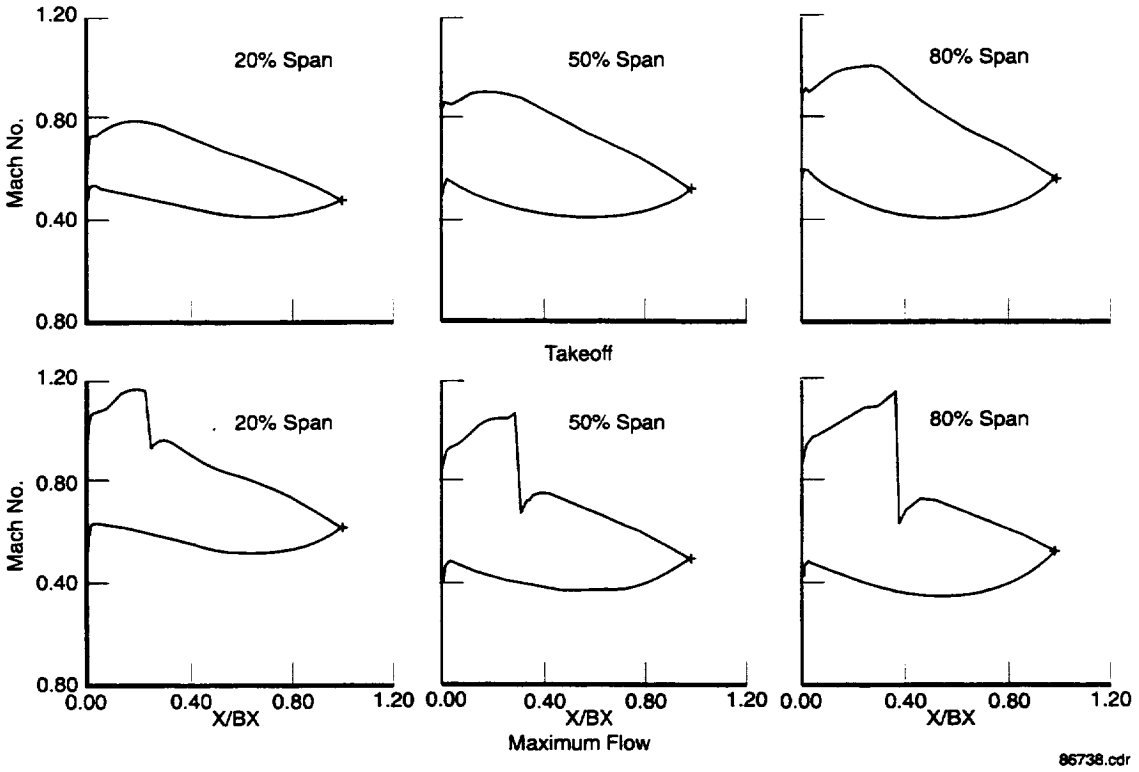

Figure 9. Fan Off Design 2-D Mach Distributions

2.5 CASING TREATMENT DESIGN

Low-Noise Fan 1 testing as well as other Pratt & Whitney (P&W) testing has verified that casing treatment can improve fan operability. The basic advanced low-noise configuration is based on these previous designs scaled to the advanced low-noise tip speed and pressure ratio. In addition, adjustable geometry is incorporated to allow determining performance and acoustic sensitivities to geometry variations. The goal is to minimize noise with acceptable operability and performance.

2.6 FEGV DESIGN

The number of fan exit guide vanes (FEGVs) was determined from the acoustic analysis presented in Section 4 of this report. The goal is to minimize noise with a realistic configuration. The aerodynamic design was optimized with Navier-Stokes analysis to remove all airfoil separations.

The initial conventional FEGV design resulted in an airfoil with no predicted separation on a 2-D basis (Figure 10). However, 3-D Navier-Stokes indicated significant separation in the outer 10-percent span. This separation is a result of the high turning requirements in a FEGV with a low tip speed fan. Using Navier-Stokes analysis to optimize the design, it was possible to remove this area of separation (Figure 11).

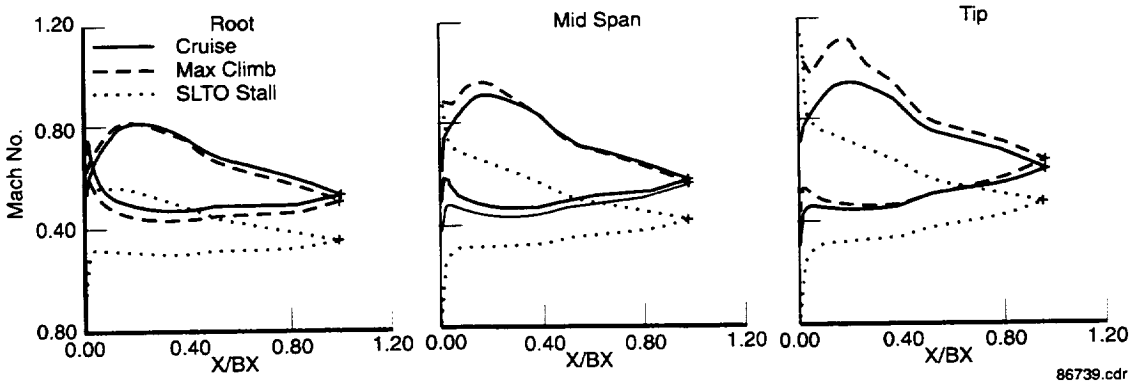

Figure 10. FEGV 2-D Blading Design Mach Contours

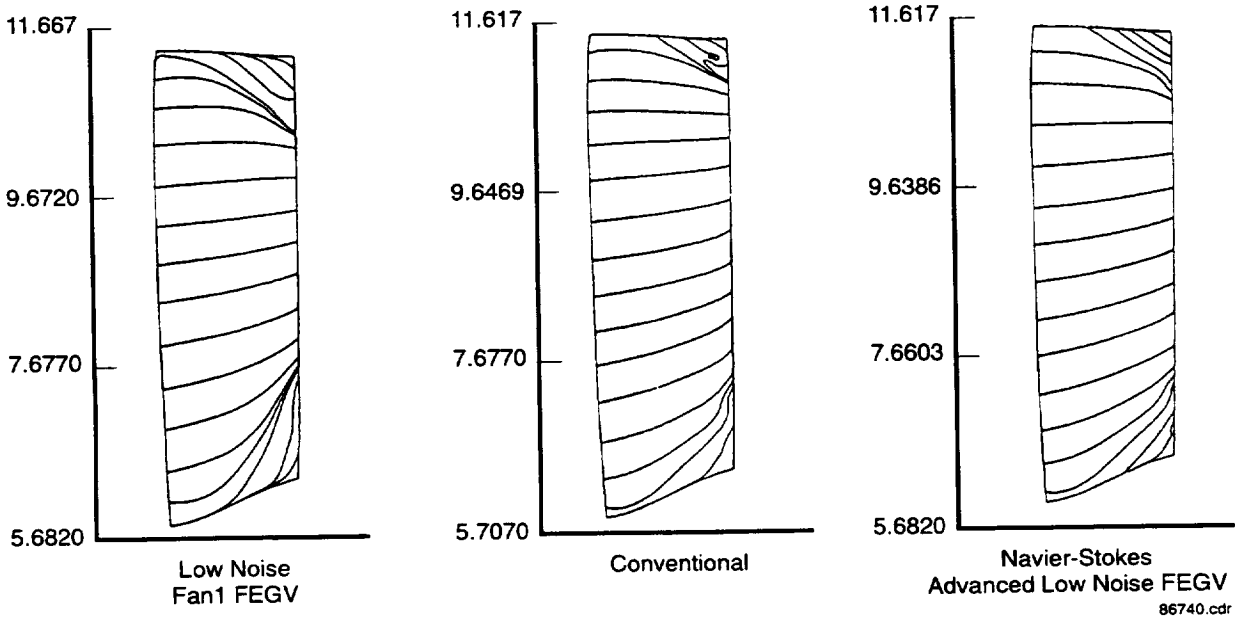

Figure 11. FEGV 3-D Suction Surface Streakline Comparisons

2.7 CORE STATOR DESIGN

A core stator design was completed for this advanced low-noise fan. Figure 12 compares the design point Mach contours of this stator to those from the current Low-Noise Fan 1 core stator. Since the two designs were so similar, it was decided not to build the new stator, but reuse the existing core stator from Low Noise Fan 1.

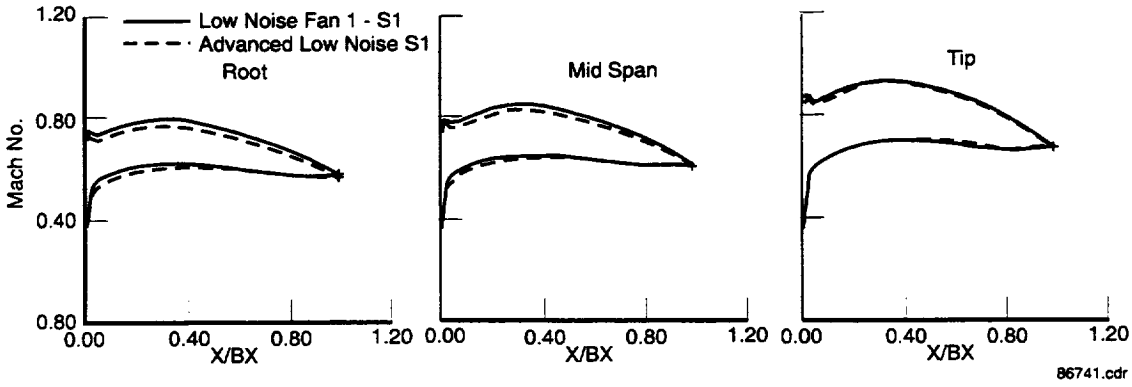

Figure 12. Core Stator Design Mach Contours

3. FAN STRUCTURAL DESIGN

3.1 FAN BLADE ANALYSIS

3.1.1 Objective

The low-noise model fan blade is designed for use in a multidisciplinary test for acoustics, aerodynamics, nacelle, and structures. The model blade features a solid titanium construction with a circular dovetail attachment to permit variable pitch capability. This section summarizes design considerations and the analyses performed to determine stress, deflection, resonance frequencies, and flutter.

3.1.2 Design Conditions

The geometric parameters, rotational speeds, and aerodynamic conditions used in the structural analyses are summarized in Table 2. Frequency analyses are performed at the minimum cruise and redline conditions. Cold airfoil geometry is defined for the cruise condition. Steady stresses are computed at maximum climb and redline rotor speeds.

Table 2. General Airfoil Information

Material	*AMS 4928*
Blade Count	18
Fan Pressure Ratio at Design Point	1.29
Flow Rate at Design Point ($lb_m ft^2/sec$)	91.8
Design Point $N_{I_{mech}}$ (rpm)	7557
Redline $N_{I_{mech}}$ (rpm)	9596
Hot Day Sea-Level Takeoff $N_{I_{mech}}$ (rpm)	8077
Minimum Cruise $N_{I_{mech}}$ (rpm)	7287
Redline Tip Speed (ft/sec)	903
Average Root Radius (in.)	4.83
Average Tip Radius (in.)	11.00
Standard Day Temperature	59°F
Hot Day Temperature	(Standard Day + 27°F)

3.1.3 Material Selection

Titanium, AMS 4928 is the fan material. AMS 4928 properties are listed in Table 3.

Table 3. AMS 4928 Material Properties at 150°F

Parameter	*Symbol*	*Value*
Density	ρ	0.160
Elastic Modulus	E	16.0^6 psi
Poisson's Ratio	v	0.160
0.2% Yield Strength	σ_{ys}	125.0^3 psi
Ultimate Strength	σ_{ult}	132.0^3 psi
Smooth Endurance Strength	σ_{endure}	45.0^3 psi

Source: Pratt & Whitney Material Test Data

3.1.4 Airfoil Finite-Element Model

The blade finite-element model was generated for use with MSC/NASTRAN Version 68.1.[1] Three element types were used to construct the model. Plates were used in the airfoil, and beams were used for the attachment. Bar elements tied the airfoil to the attachment. Air pressure loads were included using PLOAD2 cards for the design point, sea-level takeoff (SLTO), maximum climb, and redline. The finite-element model is configured for varying angles of attack corresponding to the design conditions through coordinate system rotation.

3.1.5 Blade Airfoil Steady Stress

Airfoil steady-stress levels are calculated at maximum climb and redline. Acceptable low-cycle fatigue (LCF) life is predicted for the airfoil, Appendix C. A maximum number of LCF cycles was determined using a NASA LeRC guideline, three times the number of estimated rig startup-shutdown cycles. The maximum of 1,000 cycles was estimated. A maximum nominal steady stress equal to 52.7 ksi occurred at redline. Applying stress concentration factors to the nominal steady stress at the root fillet result in a concentrated stress of 61.4 ksi and a predicted airfoil stage life greater than 1,000 cycles.

3.1.6 Blade Attachment Steady Stress

Attachment steady-stress levels peak at the redline design condition. Peak nominal stresses are 20.5 ksi, 14.1 ksi, 26.5 ksi, and 27.1 ksi for combined membrane and bending, tooth bending, tooth shear, and bearing stress, respectively. Attachment stage life is predicted to be greater than 1,000 cycles under a peak concentrated combined stress of 51.7 ksi.

3.1.7 Resonance Vibration and Flutter

Figure 13 is a Campbell diagram for the low-noise fan. The fan blade geometry provides acceptable resonance frequency characteristics. Reduced velocity flutter parameters as listed in Table 4 are acceptable by NASA LeRC compressors and turbines design criteria.[2]

[1] MSC/NASTRAN Version 68 Release Notes, © MacNeal-Schwendler Corporation, June 1994

[2] NASA LeRC Design Criteria: Compressors and Turbines, Section 1.18.8.4

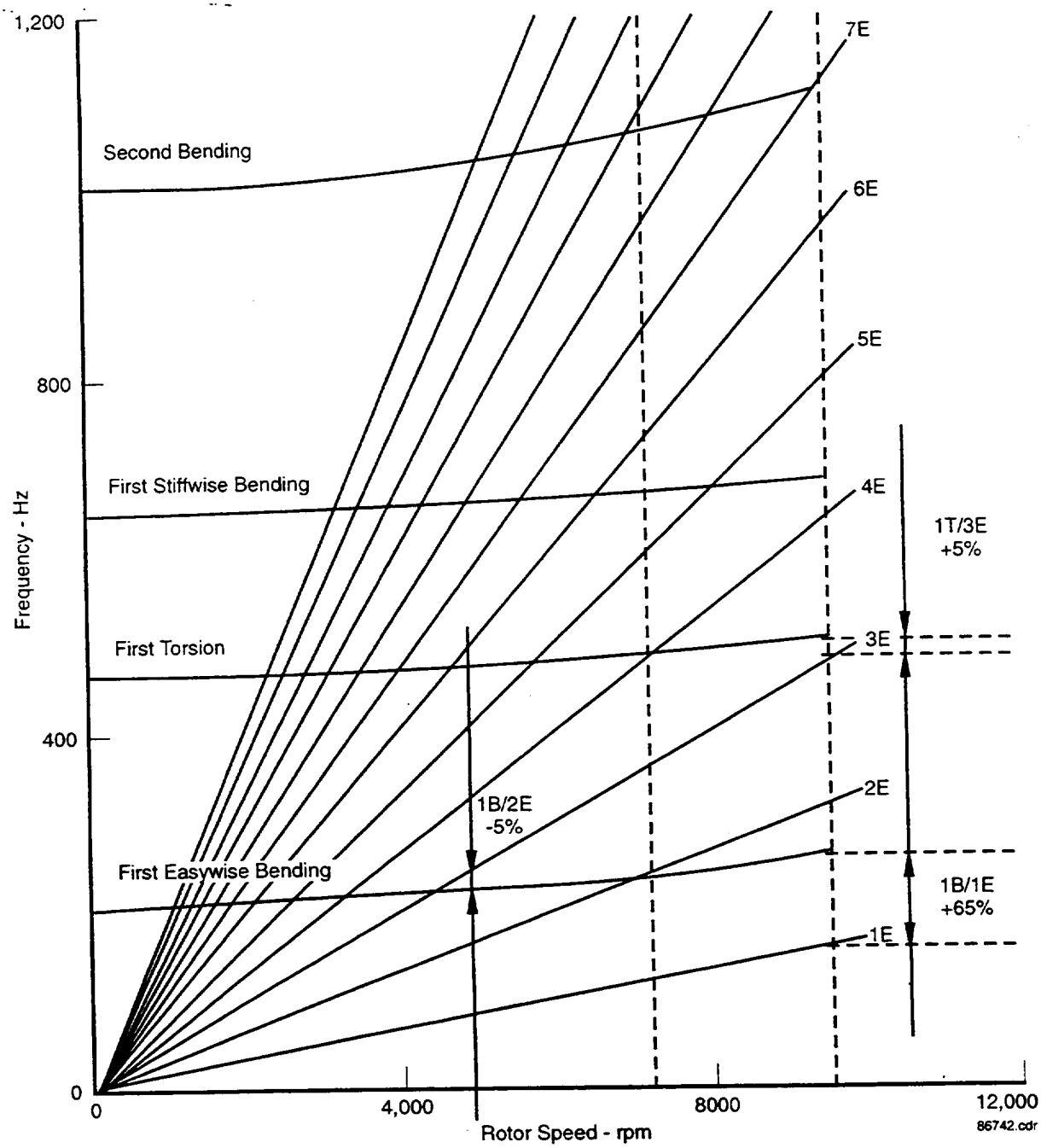

Figure 13. Low-Noise Titanium Fan 2 Geometry Campbell Diagram

Table 4. Low-Noise Advanced Ducted Propulsor Velocity Parameters

Vibratory Mode	*NASA LeRC Criteria*	*Reduced Velocities*
First Bending	6.66	3.62
First Torsion	2.40	1.78

3.2 ROTOR ANALYSIS

3.2.1 Objective

The purpose of the rotor analysis is to ensure acceptable safety factors and life for all components in the rotor assembly. A stress analysis of the spinner, forward and aft disks, seal, pitch plug, torque sleeve, and balance ring, as determined using finite-element methods, is summarized in this section.

3.2.2 Finite-Element Model

The finite-element analysis software ANSYS was used to model and analyze the rotor. ANSYS PLANE42 elements were used to build an axisymmetric model. The tie rod and retainer were modeled with plane stress elements with the appropriate thickness input. Orthotropic material properties were calculated for the holes based on the volumetric ratio of the region. The material properties for the rotor components are listed in Table 5.

Table 5. Rotor Material Properties (150°F)

Material	*Part*	F_{ty} (10^3 lb/in.^{2})	F_{tu} (10^3 lb/in.^{2})	E (10^6 lb/in.^{2})	μ_{xy}	α (10^{-6} in./in./°F)	ρ (lbf/in.^{3})
AL 2024-T4	Forward and Mid Spinner	42	61	10.5	0.33	12.8	0.101
17-4PH 1025	Aft Spinner Torque Sleeve Pitch Plug Seal Balance Ring	139	150	28.0	0.27	6.2	0.283
15-5PH 1025	Disk	139	150	28.3	0.27	6.3	0.283
TI 6-4	Receiver	125	132	16.1	0.31	5.8	0.160
AMS 5662 (Inco 718)	Disk Tie Rod	147	181	29.1	0.29	7.0	0.297

Source: MIL-HDBK-5F

3.2.2.1 Bolt Hole Region Modeling Description

Rotor hardware bolt interfaces are modeled by coupling components in the radial and/or axial directions. The torque sleeve flange is coupled in the radial and axial directions to the mid spinner. The pitch plug is coupled in the radial and axial directions to the aft spinner. The forward disk flange is coupled in the radial and axial directions to the aft spinner. The aft disk flange is coupled in the axial direction to the seal. The balance ring is coupled in the axial and radial direction to the aft disk. The torque sleeve aft flange is coupled in the axial direction to the aft disk.

3.2.2.2 Contact Region Modeling Description

Initial (preload) interferences and gaps for the rotor are included in the finite-element model. Contact elements are used to model the interferences and gaps. The preload for the disk tie rod was calculated as follows:

$$\delta = F \bullet L / A \bullet E = \sigma \bullet L / E = 0.0126 \text{ in.}$$

where δ = Axial deflection (preload interference input)

σ = $0.75 \bullet \sigma_{ys}$ @ 150°F = 147 ksi

L = Bolt length from forward disk face to aft disk face = 3.3155 in.

E = Young's Modulus @ 150°F = 29.1^6 psi

3.2.3 Constraints

The model is constrained in the axial direction at the inner diameter forward face of the balance ring.

3.2.4 Loading

The loading per blade was developed for four load cases: cruise, SLTO, maximum climb, and redline. The loads applied to the model were an axial force, radial force, moment about the hoop axis, and angular velocity. The actual loads input into the analyses are for all eighteen blades. The model was analyzed at a uniform temperature of 150°F.

3.2.5 Analysis Results

A nonlinear analysis with stress stiffening was performed for preload, cruise, SLTO, maximum climb and redline load cases.

3.2.5.1 Maximum Principal Stress

The maximum principal stresses for each component at the redline condition are summarized in Table 6. The peak stress location for the rotor for all load cases is located at the forward fillet of the aft disk T snap. The redline load case stress at this fillet is 78.6 ksi.

Table 6. Rotor Maximum Principal Stress

Component	*Redline Maximum Principal Stress (ksi)*
Spinner	21.9
Torque Sleeve	22.0
Pitch Plug	17.0
Disk	78.6
Seal	10.6
Balance Ring	25.2

3.2.5.2 Yield and Ultimate Margin of Safety

The yield and ultimate margins of safety were calculated for the worst load case: redline. The margins were calculated using the peak maximum principal stress for each component. The smallest margins of safety occur at the aft disk T snap forward fillet and are 0.77 and 0.91 for the yield and ultimate MS, respectively. Table 3.6 summarizes the margins for the redline load case.

Table 7. Margin of Safety

Component	*Yield MS (Redline)*	*Ultimate MS (Redline)*
Spinner	5.33	5.83
Torque Sleeve	5.31	5.81
Pitch Plug	7.18	7.83
Disk	0.77	0.91
Seal	12.07	13.11
Balance Ring	4.51	4.94

3.2.5.3 Low-Cycle Fatigue Life

The nominal stress value used to calculate the LCF life for each component was obtained by calculating the net section maximum principal stress at the peak stress regions. The largest net section stress occurred at the aft disk T snap region with a value of 31 ksi and a peak stress Kt = 2.53. The calculated life for the highest stress region (aft disk T snap) at the worst load case (redline) is greater than the goal of 1,000 cycles (Appendix C).

3.2.5.4 Burst Margin of Safety

The burst margin of safety was calculated using the average hoop stress for the forward and aft disks and the allowable burst stress (MS_{burst} = (F_{burst}/σ_{hoop}average)-1). The allowable burst stress was calculated using $F_{burst} = (0.7 \times F_{tys})/1.5$. The burst margin of safety for the redline load case was 2.75.

3.2.5.5 Snap Contact Surface Status

All of the snap contact surfaces with an initial interference remained in contact for all load cases. The contact surface between the forward disk and pitch plug (initial interference 0.0 in.) does not make contact.

3.2.5.6 Disk / Spinner Flow Path Split Line Radial Displacement

The radial displacements at the OD of the aft spinner and aft disk at the split line are determined for aerodynamic concerns. The radial displacement of the aft disk is greater than the aft spinner creating a step in the flow path. The largest step occurs at the redline load case (0.00055 in.).

3.2.6 Conclusions

- Margins of safety for yield, ultimate, and burst are acceptable for all load cases
- LCF life of the rotor exceeds the life goal
- Forward and aft disk remain in contact along the entire split line for all load cases
- All snaps with initial interference remain in contact for all load cases.

3.3 FAN EXIT GUIDE VANE ANALYSIS

3.3.1 Objective

The purpose of the fan exit guide vane (FEGV) analysis is to:

- Analyze the stresses in the vanes for normal, limit, and ultimate load cases
- Perform modal analysis of a single vane.

3.3.2 Finite-Element Model

The finite-element analysis software ANSYS was used to model and analyze the FEGV assembly. Two rig configurations were analyzed: bellmouth inlet and flight nacelle. These two configurations were modeled using elastic plate elements (ANSYS SHELL63 elements). The stress and displacements results reported in this analysis were calculated using these plate element models unless otherwise noted. In addition, a detailed solid model of a vane sector was modeled using 3-D tetrahedral solid elements with midside nodes (ANSYS SOLID92 elements).

3.3.2.1 Plate Element Modeling

The shell elements in the nacelle model approximately model the midplane of the structure. The aft nacelle is attached to the FEGV outer ring by a ring of plate elements. The elements throughout the model use variable thickness to better approximate thicknesses, especially for the vanes.

3.3.3 Material Selection

The FEGV material is AMS 5659 (15-5PH Stainless Steel). The material properties used for 150°F were: $E=28.2^6$ psi, $\rho= 0.283$ lb/in.^{3}, $\nu=0.27$ (MIL-HDBK-5F).

3.3.4 Constraints

The nacelle and bellmouth models are constrained at the FEGV inner ring. The forward edge is constrained in the radial direction and the aft edge is constrained in all three translational degrees of freedom.

3.3.5 Loading

Four load cases were analyzed for both bellmouth and nacelle models. A uniform reference temperature of 150°F was used for all load cases. Table 8 describes each load case. The following list describes each load:

Gravity — A 1g acceleration representing gravity.

Gas loads — Airflow pressures on the forward (concave) surface of the FEGVs. Pressures vary chordwise and spanwise.

Angle of Attack — These loads represent the inlet flow forces resulting from a 25-deg yaw angle. The forces are: 600 lb to the left (forward lkg aft) and 100 lb aft. The forces are applied at a node on the centerline forward of the inlet and distributed rigidly to the nacelle inlet. The forces are distributed to the inlet using constraint equations.

Stall Pressures — Surface pressures on internal hardwall between fan rotor and FEGVs along the right hand side (forward lkg aft) from top dead center to bottom dead center (BDC).

Rub Forces — This load models the effects of the fan rubbing against the internal walls at the fan stacking line. The forces are applied tangentially along right hand inner side (forward lkg aft) over a 90-deg span (225 through 315 deg). The forces increase counterclockwise (ccw) in a sinusoidal manner. The total torque about the centerline = 27,200 in-lb.

Impact Load — This load models a blade striking the inner wall at the fan stacking line. An 8600-lb force is applied radially outward at BDC.

Table 8. FEGV Load Case Description

Model Description	*Load Case*	*Gravity*	*Gasloads*	*Angle of Attack*	*Stall Pressures*	*Rub Forces*	*Impact Force*
Nacelle	Gravity	✓					
Bellmouth	Gravity	✓					
Nacelle	Normal	✓	✓	✓			
Bellmouth	Normal	✓	✓				
Nacelle	Limit	✓	✓	✓	✓	✓	
Bellmouth	Limit	✓	✓		✓	✓	
Nacelle	Ultimate	✓	✓	✓	✓	✓	✓
Bellmouth	Ultimate	✓	✓		✓	✓	✓

3.3.6 Analysis

Elastic linear static stress analyses were performed for the four load cases described previously.

3.3.6.1 Gravity Load Case

The gravity load case was run as a check to help verify the model and post-processing.

3.3.6.2 Normal Load Case

The gasloads on the vanes causes a ccw rotation of the nacelle about the centerline. This displacement causes tensile stresses on the inner diameter of the vanes. For the nacelle model, the 600-lb angle of attack (AOA) load creates bending about the nacelle vertical axis. This bending increases the stresses on the trailing edge of the right side vanes (forward lkg aft). The maximum principal stress for the FEGVs is: Bellmouth = 36 ksi, Nacelle = 46 ksi.

3.3.6.3 Limit Load Case

The effects of the rub forces dominate the limit load case stress results. These tangential forces significantly increase the nacelle ccw rotation about the centerline and thus increase the bending stress on the vane inner diameter. The peak stress for each vane is fairly constant for the vanes of the bellmouth model. The nacelle model stress results are similar to the bellmouth with increased stresses on the right side vanes due to the load. The stall pressure does not appear to have a large impact on the peak stress in the vane due to the close proximity of the load to the vane. The maximum principal stress for the FEGVs is: Bellmouth = 108 ksi, Nacelle = 115 ksi.

3.3.6.4 Ultimate Load Case

The ultimate load case loads are the same as the limit load case with the exception of the impact force. The impact force causes the nacelle to rotate about its horizontal axis and thus imposes more bending on the vanes in the region of TDC and BDC. The maximum principal stress for the FEGVs is: Bellmouth = 140 ksi, Nacelle = 149 ksi.

3.3.6.5 Ultimate Load Case — Sector Model

The peak stress for all of the load cases is highly localized and the plate element mesh in this concentrated stress region is relatively coarse for such a large stress gradient. Therefore, a detailed solid element sector model of one vane was created to better analyze the stress concentrations in the vane. The sector model also contains the fillets that the plate model lacked. The displacements at the vane sector *cut* planes from a plate element model analysis were applied to the sector model for the ultimate load case. The resulting stress distribution is very similar to the plate element analysis. The peak stress of the sector model (157 ksi) is 5 percent greater than the plate element model.

3.3.6.6 Stress Results Summary

The peak vane maximum principal stress is listed in Table 9 for each load case. Membrane and bending stresses are calculated using the maximum principal stress. This assumes that the radial stress component dominates the maximum principal stress.

Table 9. Stress Results (psi)

Model	*Loadcase*	*Max Principal Stress*	*Membrane Stress*	*Bending Stress*
Nacelle	Normal	46,165	36,454	9,711
Bellmouth	Normal	35,919	25,846	10,073
Nacelle	Limit	115,316	83,853	31,463
Bellmouth	Limit	108,448	76,528	31,920
Nacelle	Ultimate	148,636	118,299	30,337
Bellmouth	Ultimate	139,942	103,898	36,044

3.3.6.7 Margin of Safety Summary

The yield margins of safety are summarized in Table 10. The stress values used for the normal and limit load cases are the concentrated maximum principal stress for the peak stress vane.

Table 10. Yield Margin of Safety

	Load Case		Margin of Safety	
Model	Normal (ksi)	Limit (ksi)	Normal	Limit
Nacelle	46	115	2.02	0.21
Bellmouth	36	108	2.86	0.29

The ultimate margins of safety are summarized in Table 11. The stress values used for the ultimate load case are the concentrated maximum principal stress for the peak stress vane. The peak stress region in the vane is highly concentrated.

Table 11. Ultimate Margin of Safety

Model	Elements	Load Case Ultimate (ksi)	Margin of Safety
Nacelle	Plate	149	0.01
Nacelle	Solid	157	-0.05
Bellmouth	Plate	140	0.07

3.3.6.8 Low-Cycle Fatigue

The stress results from the normal loadcase were used to calculate fatigue life. The net section stress is the averaged stress from the nodes along 25 percent of the total chord length of the FEGV, starting at the concentrated stress region (trailing edge root). This net section stress was then multiplied by the fillet Kts ($K_{tmembrane}$ = 1.38, $K_{tbending}$ = 1.18).

The calculated life for the highest stress region at normal operating loads is greater than the goal of 1,000 cycles. Table 12 summarizes the results.

Table 12. Low-Cycle Fatigue Life

Model	*Total Calculated Stress (ksi)*	*Life (cycles)*
Nacelle	41	>1.000
Bellmouth	26	>1.000

3.3.7 Modal Analysis

The modal analysis consisted of one FEGV vane fixed in all degrees of freedom at all the nodes along the inner and outer platforms. The first ten modes are summarized in Table 13.

Table 13. FEGV Modal Frequencies

Mode	*Frequency (cycles/sec)*
1	1,364
2	1,950
3	3,419
4	4,041
5	5,964
6	6,429
7	7,279
8	8,570
9	9,267
10	9,354

3.3.8 Conclusions

- The linear analysis predicts a small negative margin of safety for the ultimate load case. However, this analysis does not account for the effects of plastic deformation in the concentrated stress region of the FEGV. A plastic analysis would more accurately model the vane stresses for this loadcase. This analysis would most likely show that the highly concentrated stress would redistribute to create an overall lower concentrated stress. Only ten of the vanes show concentrated stresses greater than yield strength for this loadcase.
- Margins of safety for yield are acceptable for normal and limit load cases.
- The LCF life of the FEGVs exceeds the life goal.

4. FAN STAGE ACOUSTIC DESIGN

4.1 OBJECTIVE AND APPROACH

The Task 49 objective was to design an advanced model low noise fan stage to be used in combined acoustic and aerodynamic fan and nacelle testing. The stage design was to be based on the low noise stage design completed and tested in Task 2 and 31 under NAS3-26618 and fit within the existing model nacelle.[3] The existing model is a 22-in. (.56m) fan diameter scale model of an advanced ducted propulsor (ADP) concept achieving substantial noise reduction through low fan speeds relative to current turbofans. The objective of this subtask was to provide a coordinated acoustic design input to the aerodynamic design of the advanced low noise fan stage design, hereafter referred to as Fan 2. This fan stage design was to provide additional noise reduction relative to the low-speed fan stage design, referred to as Fan 1, recently completed under the aforementioned contract. The design was to be based on the 18-blade rotor, 45-vane fan exit guide vane (FEGV), 63-core inlet stator, Fan 1 design and include the fan, advanced fan tip casing treatment, FEGV, and core inlet stator. The FEGV assembly provided the structural support for the nacelle as there were no intermediate case struts in this design. The goal was to obtain a 10-percent tip speed reduction relative to Fan 1 with a corrected tip speed of 756 fps at sea-level takeoff (SLTO), 650 fps at cutback and 469 fps at approach. The fan pressure ratio was to be 1.284 ± 0.005 at SLTO and 1.294 ± 0.005 at cruise. The aerodynamic design was to have higher aerodynamic loading and include 3-D Navier-Stokes optimized blading and advanced fan tip casing treatment. The aero design was to be closely coordinated with acoustic analysis methods and criteria to produce airfoil shapes, spacing, and numbers to provide an optimized low noise, aerodynamic design.

The design process resulted in a recommended vane number of 51 FEGVs achieving a reduction in fan noise due to vane number alone of 1.1 EPNdB (cumulative at three conditions) relative to the Fan 1 stage with 45 vanes. The expected reduction in fan noise due to the 10 percent reduction in tip speed and the new vane number should result in a cumulative noise reduction of 7.1 EPNdB relative to Fan 1.

The approach to optimize vane number follows:

1. Predict tone power levels from the rotor wake interaction with the FEGVs and core inlet stators as a function of speed and vane number
2. Calculate tone Δs relative to 18-blade fan and 45-vane FEGV
3. Use existing data from the 22-in. (0.56m) ADP fan/nacelle model with Fan 1 as a database to apply the tone Δs as a function of vane number at the three acoustic design conditions of SLTO, cutback, and approach speeds
4. Optimize the overall noise in a simulated flyover as a function of vane number.

The process to estimate the noise reduction of Fan 2 relative to Fan 1 was as follows:

1. Use the Fan 1 (hardwall with the fan tip casing treatment) levels for SLTO, cutback, and approach flight conditions as a baseline level.
2. Using a $50*\log_{10}$ (tip speed ratio) relationship between fan tip speed and noise level, apply Δs to baseline levels for a 10-percent tip speed reduction at each condition. The noise level metric is the EPNL of fan noise alone of static data projected to flight. The $50*\log_{10}$ (tip speed ratio) relationship is based on Pratt & Whitney (P&W) experience.
3. Apply the Δ for optimum vane number.

[3] Hobbs, D.E., Malmborg, E.W., Neubert, R.J., Philbrick, D.H., *Low Noise Research Fan Stage Design*, NASA Contract Report 195382, pp 21-29, March 1995.

4. After the vane optimization study was completed, new information became available indicating fan broadband noise could increase with increasing vane number. This information was not applied to the design study, but took on significance as Fan 1 data showed fan broadband noise to be the significant contributor to the total noise. Therefore, an estimate of this Δ was applied to the Fan 2 noise estimate.

The primary effort to closely coordinate the aerodynamic and acoustic design was to use fan aerodynamic performance and geometry as input to the rotor wake/stator interaction noise prediction code prepared under Task 10 of NAS3-25952.[4] This code predicts inlet and aft in-duct tone power levels assuming a constant area duct. The code used P&W-generated fan aero performance and geometry of the Fan 2 stage as input to predict the tone power levels of the fan blade passage frequency and its harmonics as a function of rotor tip speed and the number of FEGVs. The Fan 1 stage design of 18 blades, 45 FEGVs and 63 core inlet stators was acoustically cut off for blade passage frequency at all speeds on the sea-level operating line. It was the design intent of Fan 2 to maintain that cutoff condition of blade passage frequency. Tone power levels of blade passage frequency (bpf) and four harmonics (up to 5 × bpf) were calculated for vane numbers from 11 to 79 with 63 core inlet stators, and for fan rotor tip speeds from 350 to 850 fps. Additional detail is provided in Section 4.2.

During the initial stages of the Fan 2 fan stage design, preliminary, diagnostic, and far field acoustic data were obtained from the 22-in. ADP model with Fan 1 in the NASA Lewis 9 × 15 ft Low-Speed Wind Tunnel. This provided an opportunity to use data from the same model in which the new fan stage design would be incorporated. The test installation is shown in Figure 14. Far-field acoustic data used in this analysis were obtained on a 88-in. (2.2m) sideline traversing microphone at 32 angles, and 12 speeds that included the acoustic off-design points of approach, cutback, and SLTO. A description of the data and data processing is presented in Section 4.3. Pratt & Whitney computer codes were used to separate the tones from each spectrum and store them in a separate matrix. The broadband only spectrum for each condition and angle was also stored, permitting a means to apply predicted tone Δs to the tone levels of the Fan 1 data as a function of vane number. The new tone levels were then logarithmically combined with the broadband to create a new spectrum with tone levels corresponding to different vane numbers.

The final step in the analysis calculated a simulated flyover level for each vane number at the three acoustic conditions of approach, cutback, and SLTO. The resultant calculated metric, tone-corrected perceived noise level (PNLTi), was an angle-integrated, tone-corrected, perceived noise level as a function of vane number, which is a close approximation of a flight EPNL. Each PNLTi was compared to the 18-blade, 45-vane PNLTi at each of the three conditions and Δs were established. The vane number that produced the greatest reduction in cumulative PNLTi relative to the Fan 1 45-vane FEGV was chosen.

4.2 FAN-TONE NOISE PREDICTION

The rotor/stator interaction noise prediction procedure was used to calculate fan-tone power levels generated by the interaction of the fan rotor wakes interacting with the fan exit guide vanes and the core inlet stators.[5] The theoretical formulation and philosophy of the code are discussed in a separate report by Meyer and Envia.[6]

Input for the code came from 2-D or steady, axisymmetric streamline, fan stage aerodynamic performance prediction code and geometry files generated during the fan stage design process. Recommendations from the Fan/Compressor group suggested the FEGV vanes be nominally radial. Fan aerodynamic performance suggested there may be benefit in extending the chord at the tip and incorporating some amount of circumferential lean in the tip region. Subsequent computational fluid dynamics (CFD) calculations showed the tip chord extension would actually increase flow separation on the vane, and this feature was removed from the design. Beyond that limited departure from a nominal radial design, anything more radical in terms of lean and sweep was considered as structurally

[4] Mathews, D.C., Topol, D.A., *Rotor Wake/Stator Interaction Noise Prediction Code — Technical Documentation and User's Manual*, prepared under NASA Contract NAS3-2592 (Task 10), April 1993.

[5] Ibid.

[6] Envia, E., Meyer, H.D., *Aeroacoustic Analysis of Turbofan Noise Generation*, NASA Contract Report 4715, March 1996.

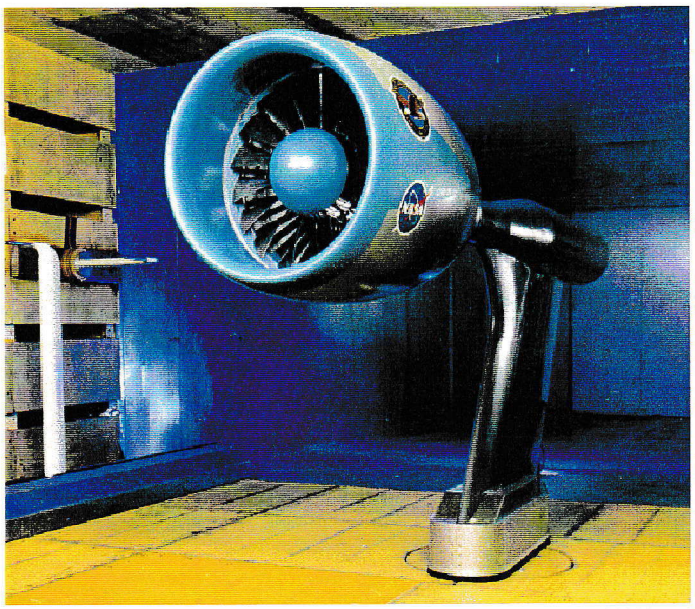

Figure 14. NASA/P&W 22-in. ADP in LeRC 9 × 15 ft Wind Tunnel

risky based on the FEGV assembly stress analysis available at the time. The small amount of tangential lean was incorporated in the tip region of the acoustic input of the prediction code. The 2-D aero and geometry files provided the input data for the simplified duct and airfoil model geometry, air angles, and mean flow conditions necessary for the fan-stage tone noise predictions. The noise prediction input files were run for a series of model speeds so the calculated tone power levels could be expressed in the output files as a function of both model speed and vane number. Cases were run for every other vane number from 11 through 79 with a constant 63 core inlet stators. The only modification to the input file made as a function of vane number was the vane chord. As vane number increased, the chord decreased proportionally to maintain constant solidity in the design. A lower vane number resulted in a longer chord. The leading edge position of the FEGV was maintained so axial spacing remained constant.

The output from the code gave the circumferential, radial, and total in-duct tone power levels for the upstream and downstream propagating modes for the rotor/FEGV interaction, the rotor/core stator interaction, and the total power level for the two interactions. The code assumed the rotor/core stator interaction propagating modes, propagated only upstream and radiated as inlet noise. The tone power levels for all propagating modes were output by individual fan harmonics. A post-processing code read the output of the tone power prediction code and stored the tone power levels as a function of speed, vane number, and fan harmonic. Thus a complete tone power level file was structured to study the behavior of the tone power levels throughout the entire range of speeds on the operating line for any given vane number, and the behavior of the tone power levels as a function of vane number at any given speed. The results were plotted and studied graphically.

Observations were first made with the blade = 18 and vane = 45 case. This was expected to be somewhat similar to Fan 1 at the three acoustic off-design conditions of approach, cutback, and SLTO, which corresponded to corrected fan tip speeds of 521, 722, and 840 fps. Observations of the Fan 1 measured data (described in Section 4.3) seemed to approximate the trends from the predictions for Fan 1 and the Fan 2 predictions for the blade = 18 and vane = 45 case. Figures 15 and 16 show the Fan 2 predicted total inlet (rotor/FEGV and rotor/stator interactions) and aft power levels for fan harmonics 2 times blade passage frequency (2bpf) through 5bpf as a function of tip speed. Figures 15 and 16 also show that after the (-9,1) acoustic mode cuts on, 2bpf will contribute significantly to the aft radiated noise above 450 fps tip speed. The significant rise in 2bpf and 3bpf around 450 fps is a result of the

(-9,1) mode just cut-on. The 3bpf becomes significant at 650 fps, and 3bpf aft shows progressive radial modes cutting on as a function of speed. Additional comments about these observations, and observations made from measured data, are discussed in Section 4.3.

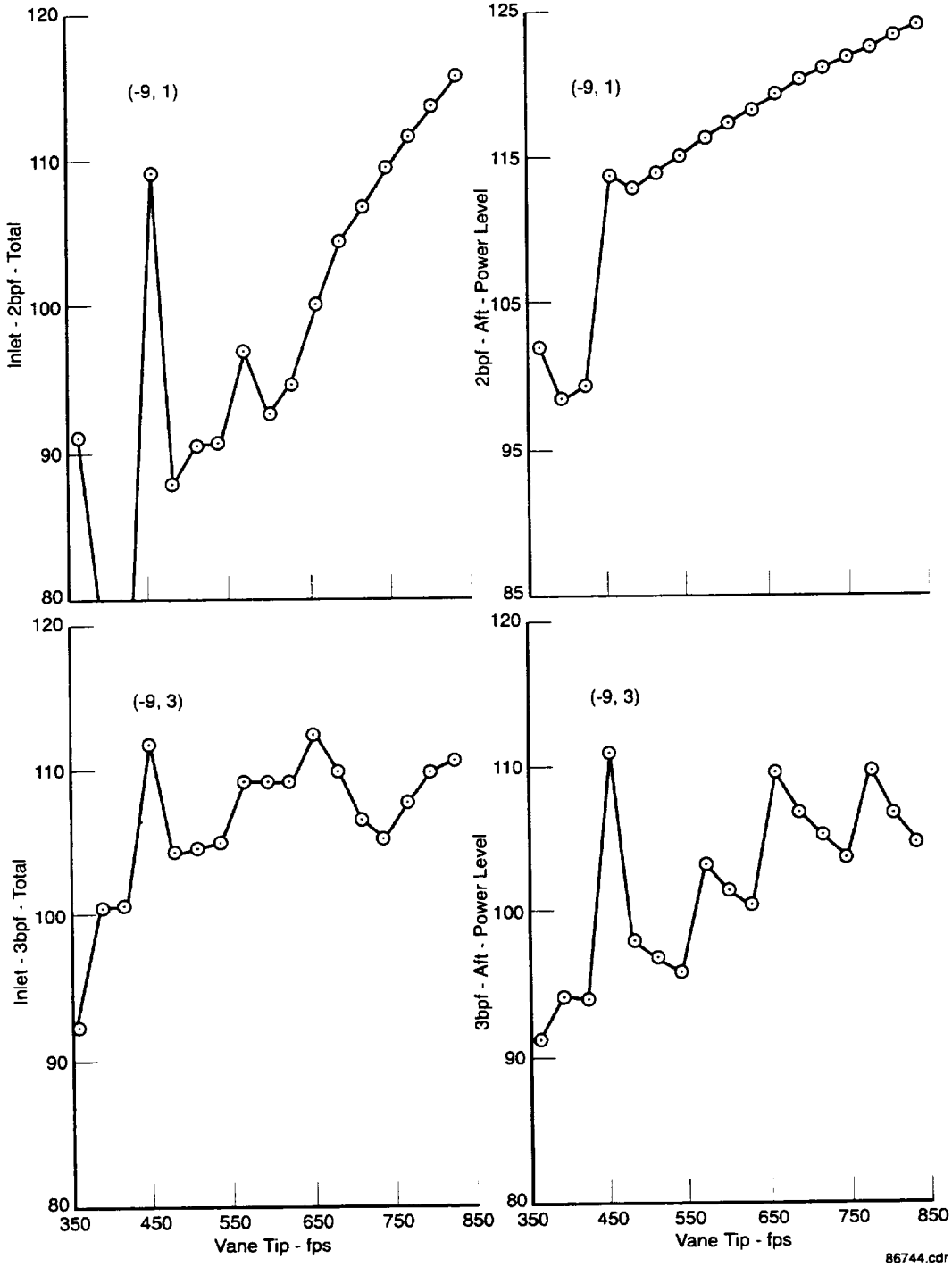

Figure 15. Fan-Tone Power-Level Predictions Advanced Low-Speed Fan (Fan 2) 2bpf and 3bpf for Blade = 18, Vane = 45 Versus Fan Tip Speed

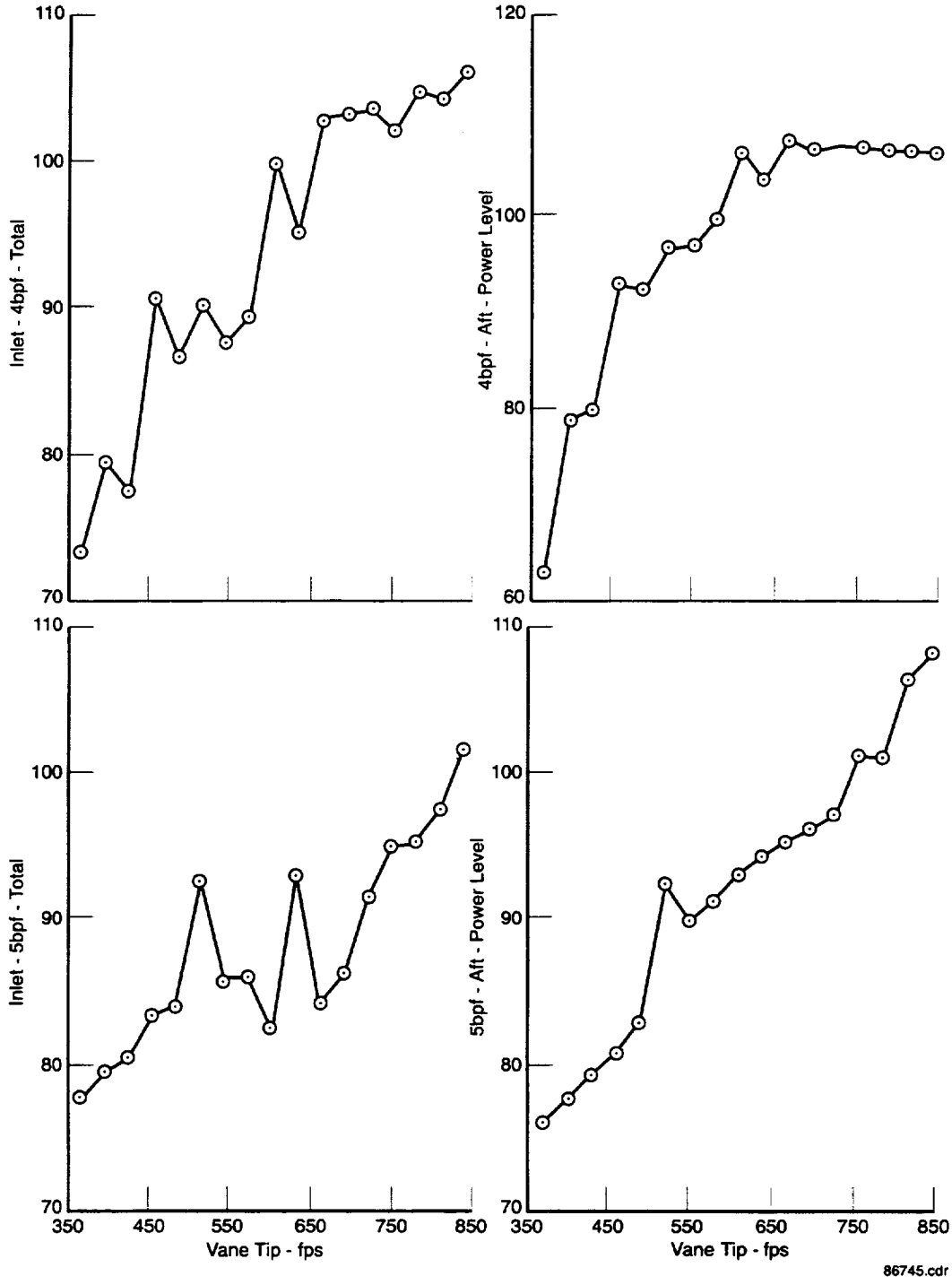

Figure 16. Fan-Tone Power-Level Predictions Advanced Low-Speed Fan (Fan 2) 4bpf and 5bpf for Blade = 18, Vane = 45 Versus Fan Tip Speed

4.3 DESCRIPTION OF 22 IN. ADP MODEL FAN 1 DATA PROCESSING

The data used in this study were digitally processed with a 59 Hz bandwidth filter and data from 234 Hz to 41250 Hz in model scale were put into a 700 spectral line matrix of sound pressure level of frequency and angle. Angle was measured from the inlet centerline. These data were adjusted from sideline measurement in the tunnel to 1 ft (0.3048 m), lossless day, data. The data were then amplitude and frequency-scaled to a full-scale engine size and extrapolated to a uniform radius. The extrapolated data were corrected for atmospheric absorption at FAA standard day conditions of 77°F and 70 percent relative humidity.

The full-scale narrowband data were noise source separated into fan-tones and fan broadband components. (The data were expected to contain fan noise only.) A code developed at P&W was used for this process. The code identified fan-tone frequencies based on number of fan blades and the mechanical rotor speed of the model at each data point condition. Then it *searched* at lower to higher frequencies around the calculated frequency in the spectrum for a fan-tone. A fan tone was identified and isolated by the application of mathematical rules governing the change in level of successive spectral lines. The broadband level at the tone and elsewhere in the spectrum was thus determined as any part of the spectrum not identified as a fan-tone and the interpolated level of broadband on either side of an identified tone. If successive spectral lines did not increase and decrease according to the predetermined rules relative to the broadband, the code indicated that no fan-tone was present and assigned a level of 0.0 to that particular tone. When the rules were satisfied indicating a fan-tone was present, the sound pressure level of the broadband *under* the tone was logarithmically subtracted from the logarithmic sum of any spectral lines making up the tone. Thus, a fan-tone matrix was created consisting of zeroes where no tones were present and tone-only sound pressure levels where they were present. The fan-tone-only matrix and the broadband definition-only matrix were stored in a database separately. The scaled, extrapolated and separated narrowband data were then converted to one-third octave band (OB) using an analogue filter shape (conforming to the International Standard filter shape described in IEC-225) developed at P&W. The fan-tone only matrix was identical in format to the one-third octave band matrix for the broadband-only noise. The tones were stored in the appropriate one-third octave bands and band sharing values were calculated conforming to the filter shape, when any tone was at the edge of a one-third octave band. The logarithmic sum of these two matrices would equal the measured spectrum. The tone only matrices were prepared for the application of the tone level Δs calculated from the procedures described in Sections 4.2 and 4.4.

The narrowband data and the one-third octave band data from the three Fan 1 test points were reviewed. The three conditions of approach, cutback, and SLTO were studied, which corresponded to corrected fan tip speeds of 521, 722, and 840 fps. This was done to see the relative importance of fan-tones and fan broadband in the spectra and identify what tones generated by the rotor wake/stator interaction from the 18-blade fan and 45-vane FEGV were the most significant. A tone was considered significant when the tone sound pressure level exceeded the broadband sound pressure level by more than 3 dB in the one-third octave band spectrum. These results indicated that 2 times blade passage frequency (2bpf) and 3bpf were significant at the approach condition in the inlet quadrant and 2bpf was significant the aft quadrant (Figures 17 and 18). Tones typically were not significant in the inlet angles at the cutback and SLTO conditions (Figures 19 and 20). 2bpf was significant in the aft angles at the cutback and the SLTO conditions, as shown in Figures 21 and 22. The vane number optimization process for Fan 2 would consider 2bpf as an important tone to attempt to reduce relative to the blade = 18, vane = 45 count of Fan 1. Additionally, the review showed the scaled fan broadband noise peaked in the frequency range of 500 Hz to 2500 Hz while 2bpf was 500 Hz or below at all three conditions. Therefore, broadband was viewed as contributing more significantly to an Effective Perceived Noise Level as would be measured and calculated in flight than the tones. This was considered consistent with previous tone and broadband sensitivity studies for Advanced Ducted Propulsor model and full scale engine data. However, the analysis proceeded with the objective of reducing overall noise by reducing the fan-tone levels with an optimum number of FEGVs. As mentioned in the previous section, similarities in the measured data and the predicted data for blade = 18, and vane = 45, added confidence to the fan-tone power-level prediction procedure and the approach for this analysis.

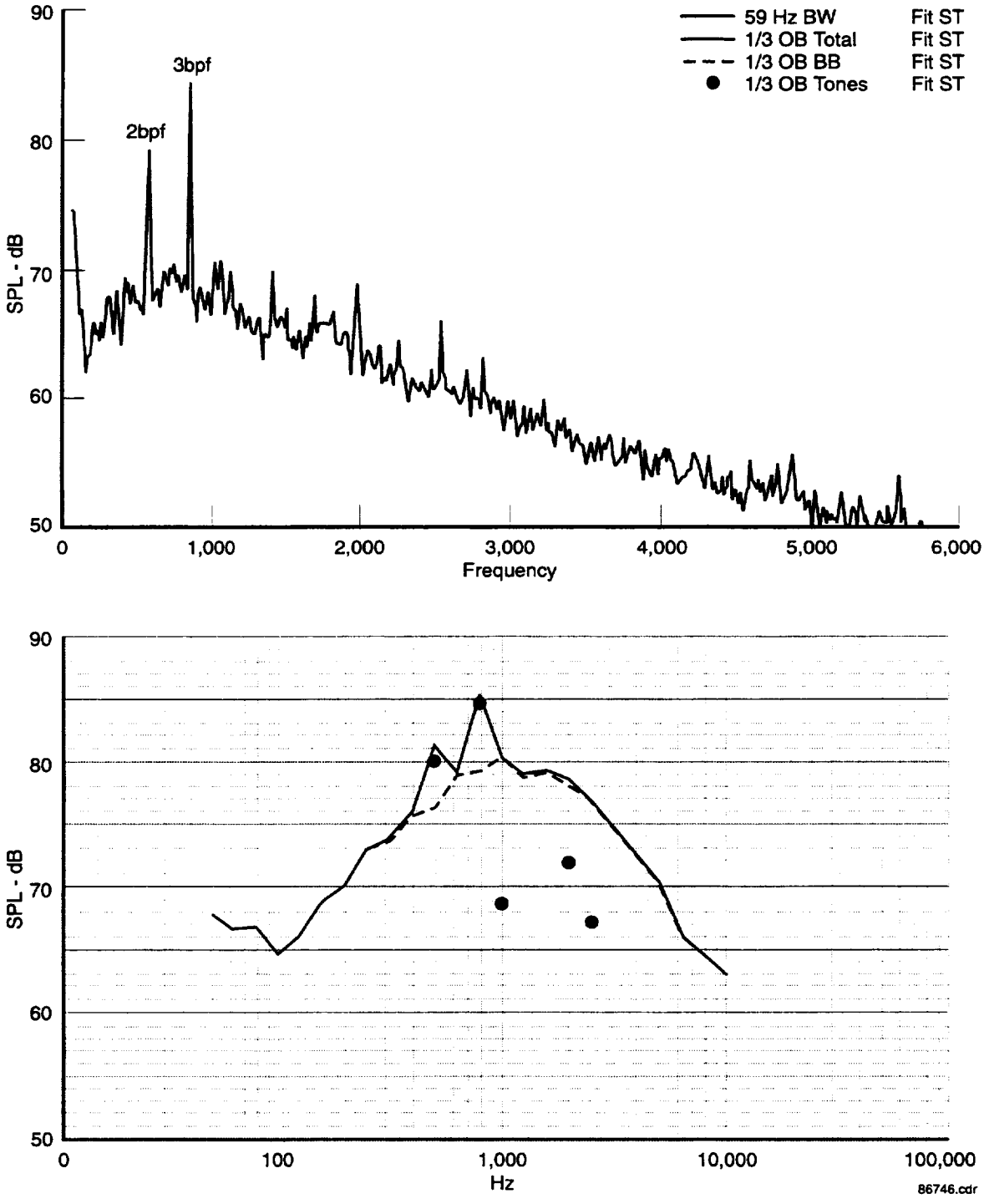

Figure 17. Low-Speed Fan (Fan 1) Narrowband and One-Third OB Spectra
47-deg Approach Condition Inlet Angle

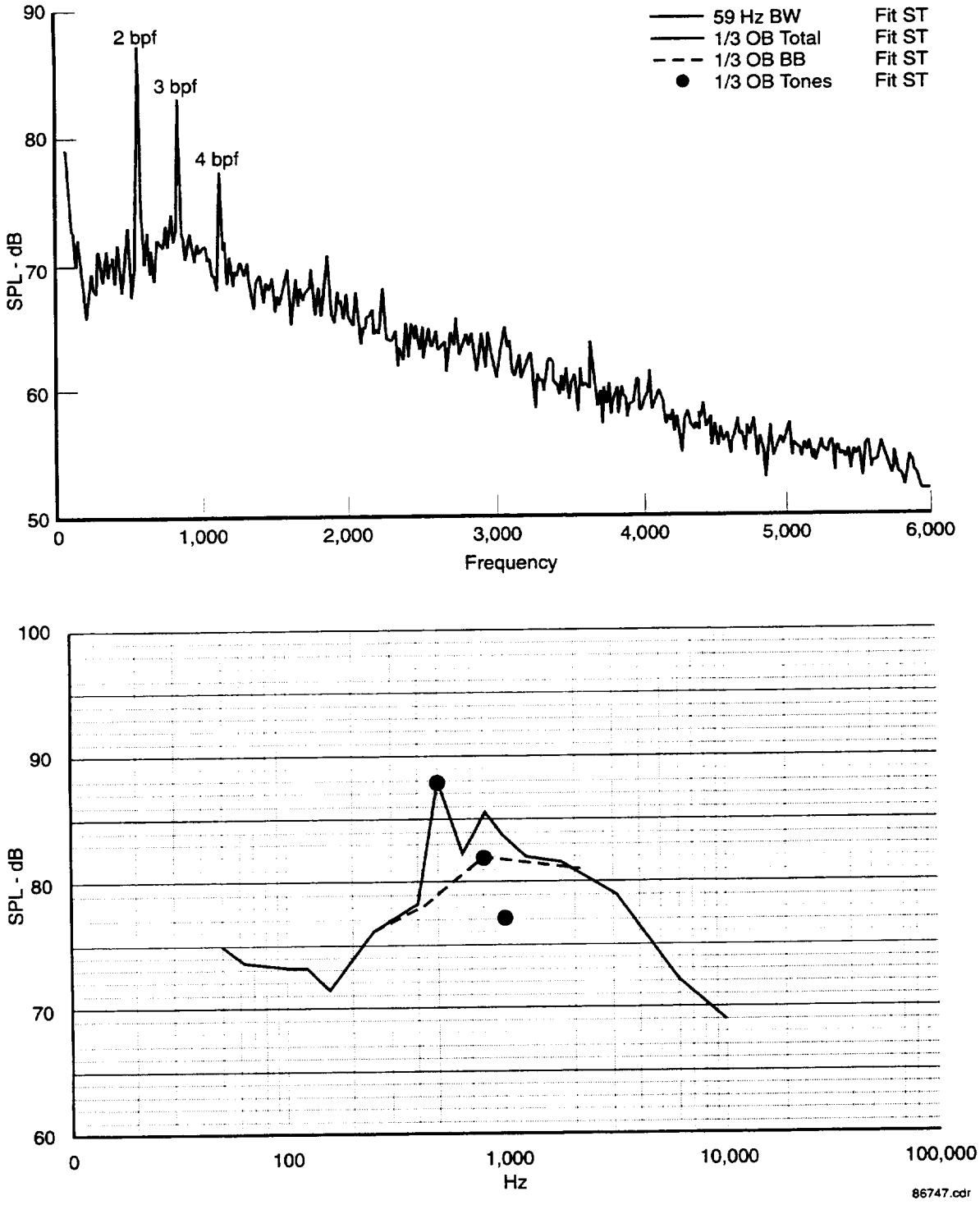

Figure 18. Low-Speed Fan (Fan 1) Narrowband and One-Third OB Spectra 130-deg Approach Condition Inlet Angle

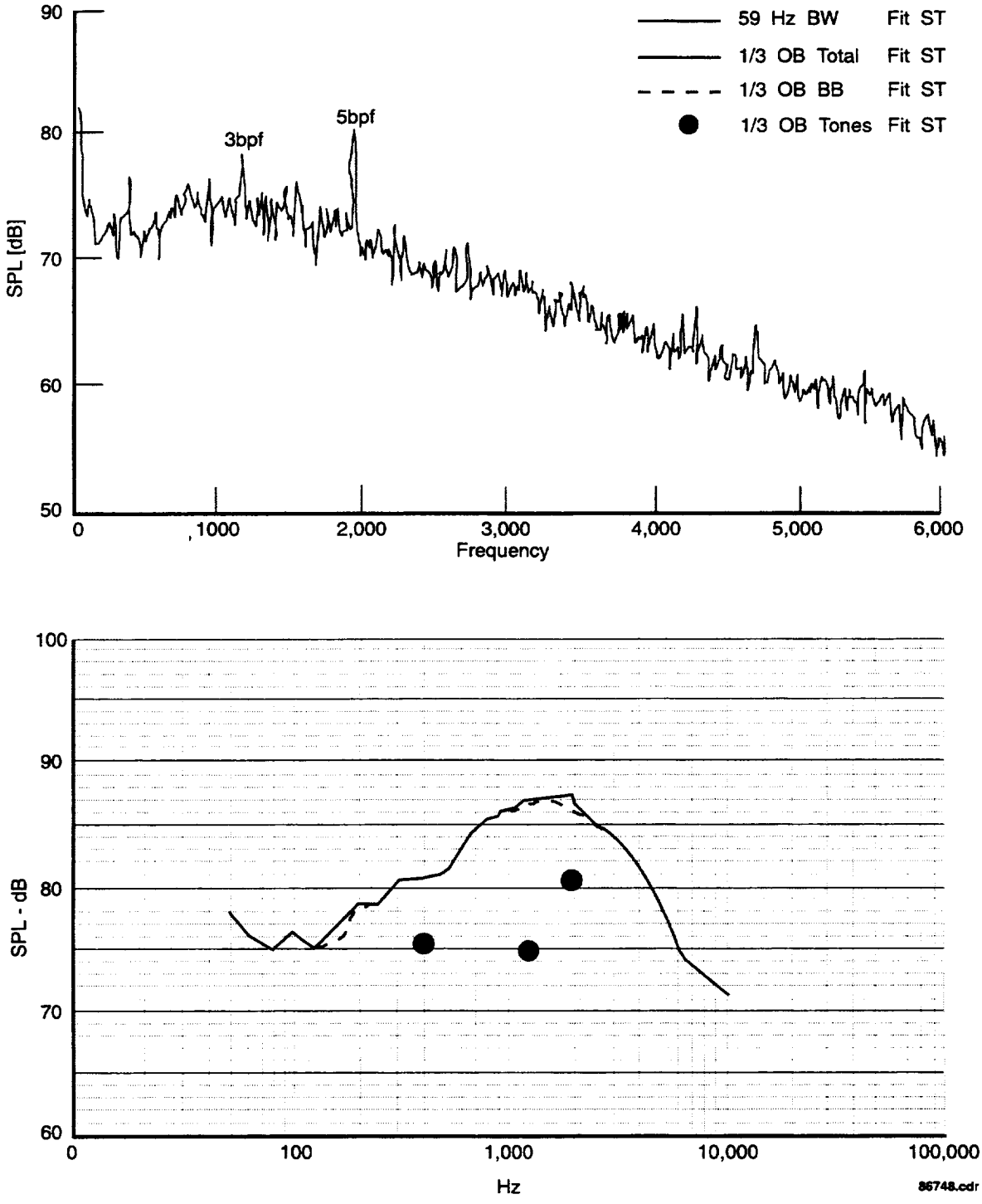

Figure 19. Low-Speed Fan (Fan 1) Narrowband and One-Third OB Spectra
56-deg Cutback Condition Inlet Angle

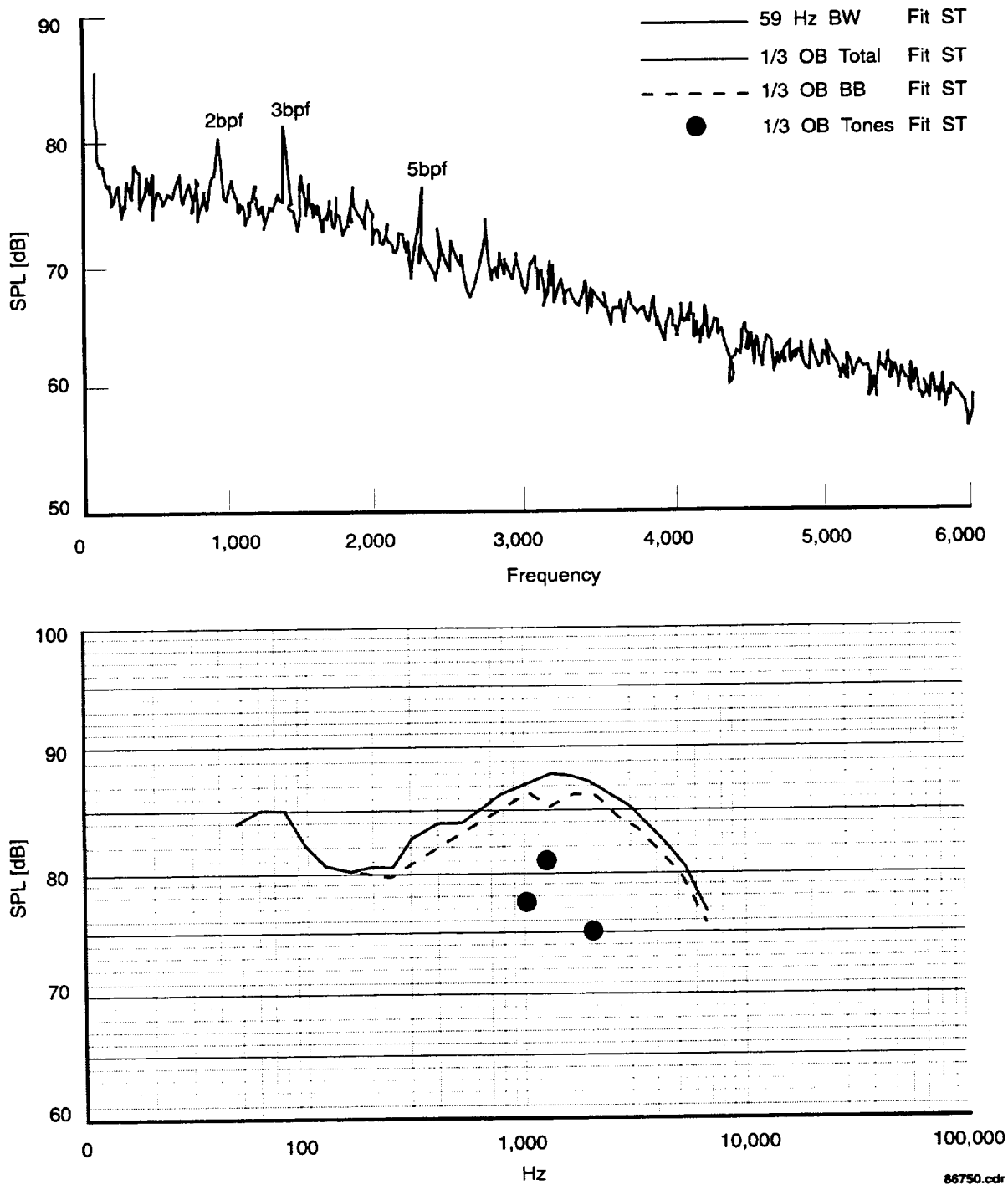

Figure 20. Low-Speed Fan (Fan 1) Narrowband and One-Third OB Spectra
56-deg SLTO Condition Inlet Angle

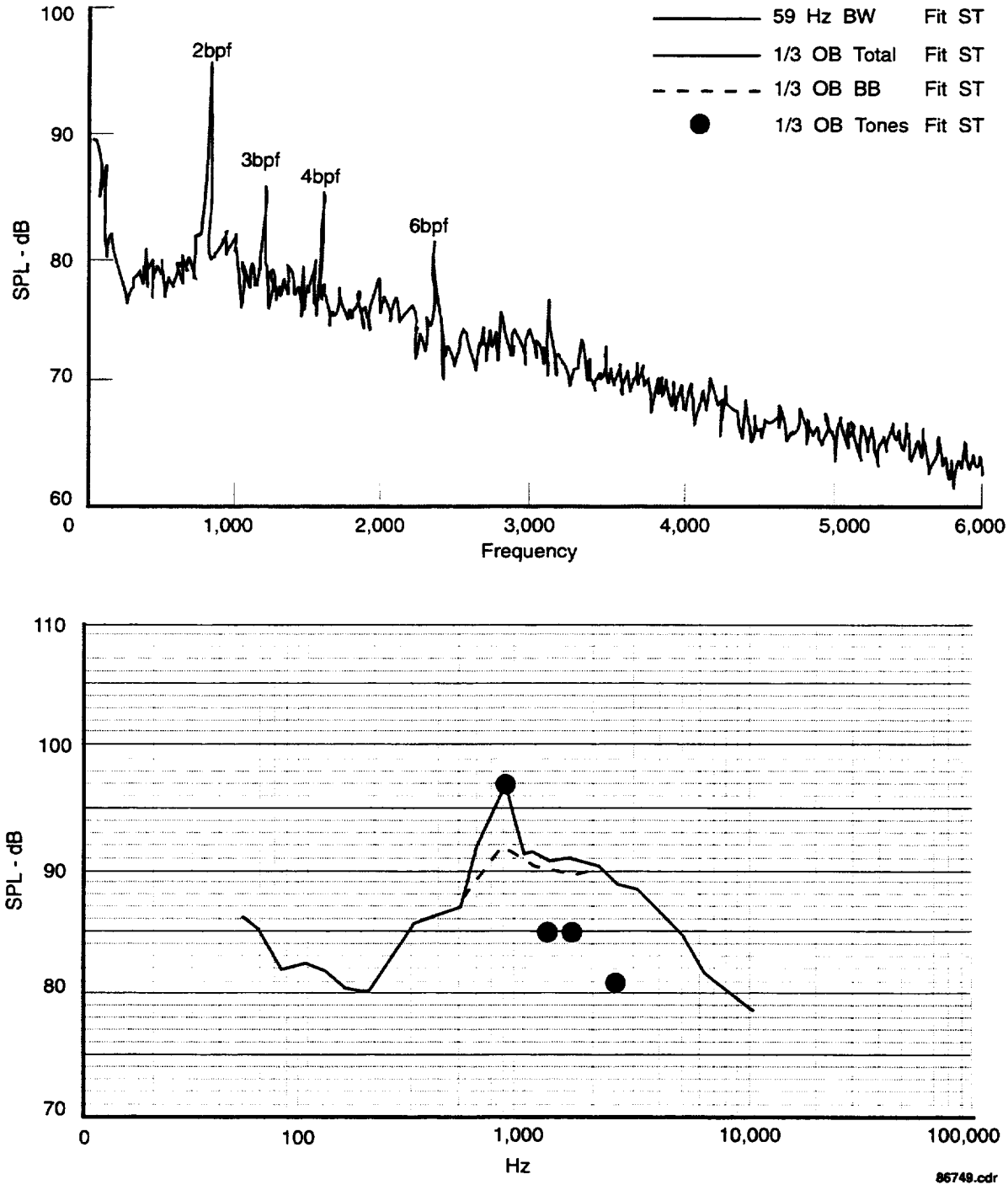

Figure 21. Low-Speed Fan (Fan 1) Narrowband and One-Third OB Spectra 130-deg Cutback Condition Aft Angle

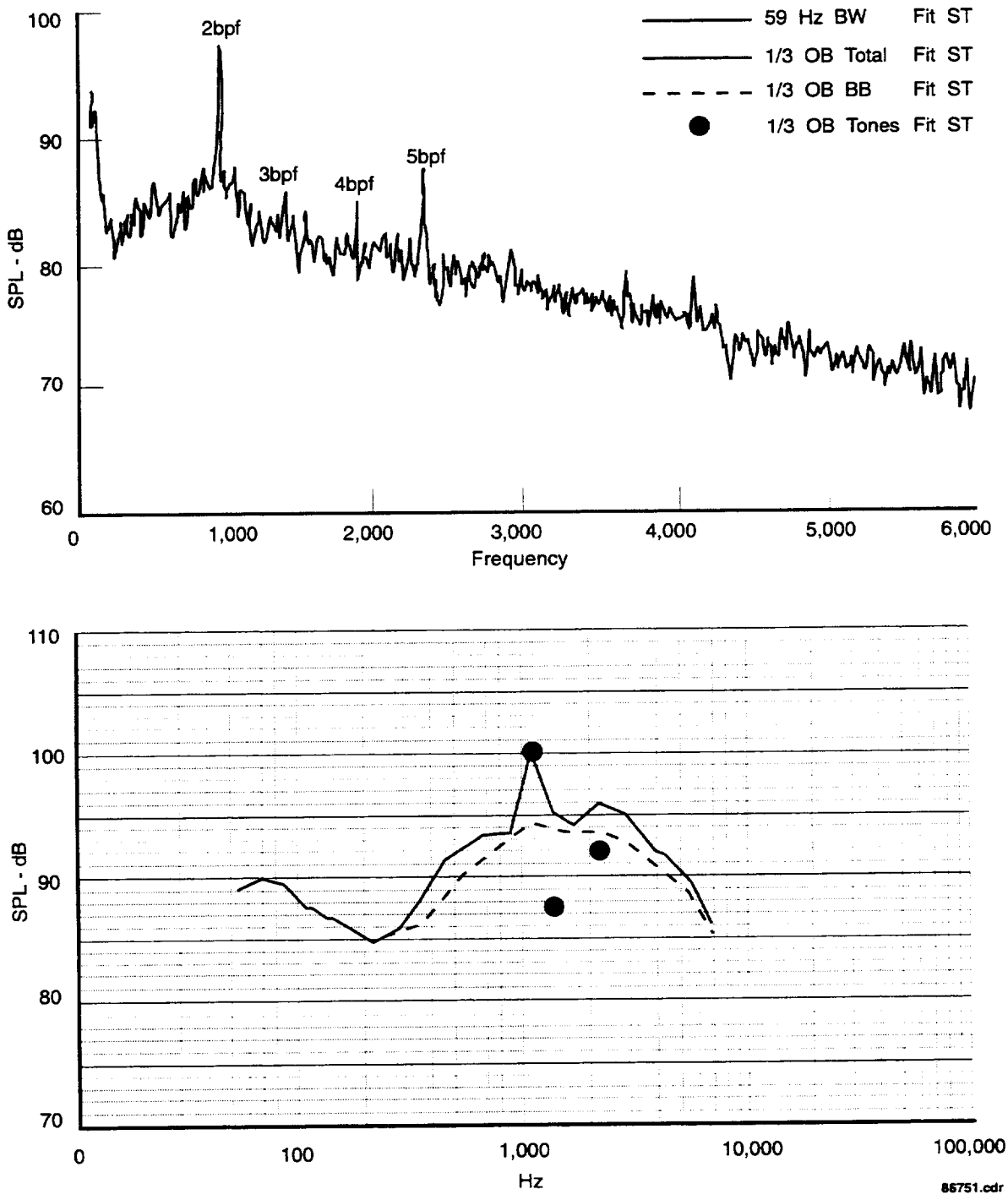

Figure 22. Low-Speed Fan (Fan 1) Narrowband and One-Third OB Spectra 120-deg SLTO Condition Aft Angle

4.4 APPLICATION OF TONE PREDICTIONS TO DATA

Section 4.2 described the prediction of in-duct tone power levels as a function of model speed and vane number from the output of the Rotor Wake/Stator Interaction Prediction Code. The predictions were in-duct power levels and thus required a means to apply the Fan 2 tone power-level Δs to the far field sound pressure level data of Fan 1. A simplifying assumption was made to expedite the design process. All tone power-level Δs, relative to the 18-blade, 45-vane case, were assumed to be equally distributable to all the far field angles. The inlet tone power-level Δs were applied to the inlet angles of 24 to 80 deg, and the aft tone power-level Δs were applied to the aft angles greater than 80 deg for the approach condition and greater than 70 deg for the cutback and SLTO condition. This assumption did not precisely account on an angle-by-angle basis, the differences in the directivities of the various cut on modes, but was considered reasonable and applicable to all modes equally in the far field.

Plots were made of the predicted tone power levels for two or three speeds near each of the three speeds at the acoustic flight conditions of approach, cutback, and SLTO as a function of vane number. Trends were observed along with the detailed prediction output, to note where specific modes were cutting on or off, the relative levels of the fan harmonics, and how sensitive the tone power levels were to vane number. Figures 23 and 24, 25 and 26, and 27 and 28 show those plots as a function of vane number. Inlet-total (FEGV and core stator combined) data are displayed on the left hand side of the plot and aft data are displayed on the right hand side of the plot.

Some observations from the plots are summarized:

- *Approach* — 2bpf cuts off at about vane = 47; 3bpf has low levels at vane = 37 and peaks at Fan 1 vane = 45; 4bpf has minimums at about vane = 51; and 5bpf has generally low levels relative to the other harmonics.
- *Cutback* — 2bpf cuts off at about vane = 57; 2bpf aft and 3bpf inlet peak at about the Fan 1 vane = 45; 2bpf inlet peaks at about vane = 32; the higher harmonics are generally lower in level.
- *SLTO* — 2bpf cuts off at about vane = 59; 2bpf aft peaks again at the Fan 1 vane number = 45; 3bpf inlet is lowest at vane = 71 and 3bpf aft is lowest at about vane = 45; 4bpf and 5bpf are lower in level than 2bpf and 3bpf and not strongly dependent on vane number.

The trends from the predictions did not lend themselves to an obvious selection of optimum vane number. Interaction with the P&W Fan/Compressor and Structures group indicated the maximum vane number from a structural perspective would be about 60. It was decided to curve fit trend lines through the predictions, normalize all the levels to vane = 45, and create Δs at each of the three conditions relative to vane = 45. These normalized Δs are shown for each of the three conditions as a function of vane number in Figures 29 and 30. Inlet-total (FEGV and core combined) data are displayed on the left-hand side of the plots and aft data on the right. Observations from these plots are summarized:

For vane numbers < 45 —

- 2bpf increases significantly in the inlet and decreases with vane number in the aft
- 3bpf decreases in the inlet, but increases at cutback and SLTO in the aft
- 4bpf and 5bpf increase at approach and decrease slowly at cutback and SLTO
- 4bpf and 5bpf levels are generally 10 dB or more lower than 2bpf and 3bpf as observed from Figures 23 and 24, 25 and 26, and 27 and 28.

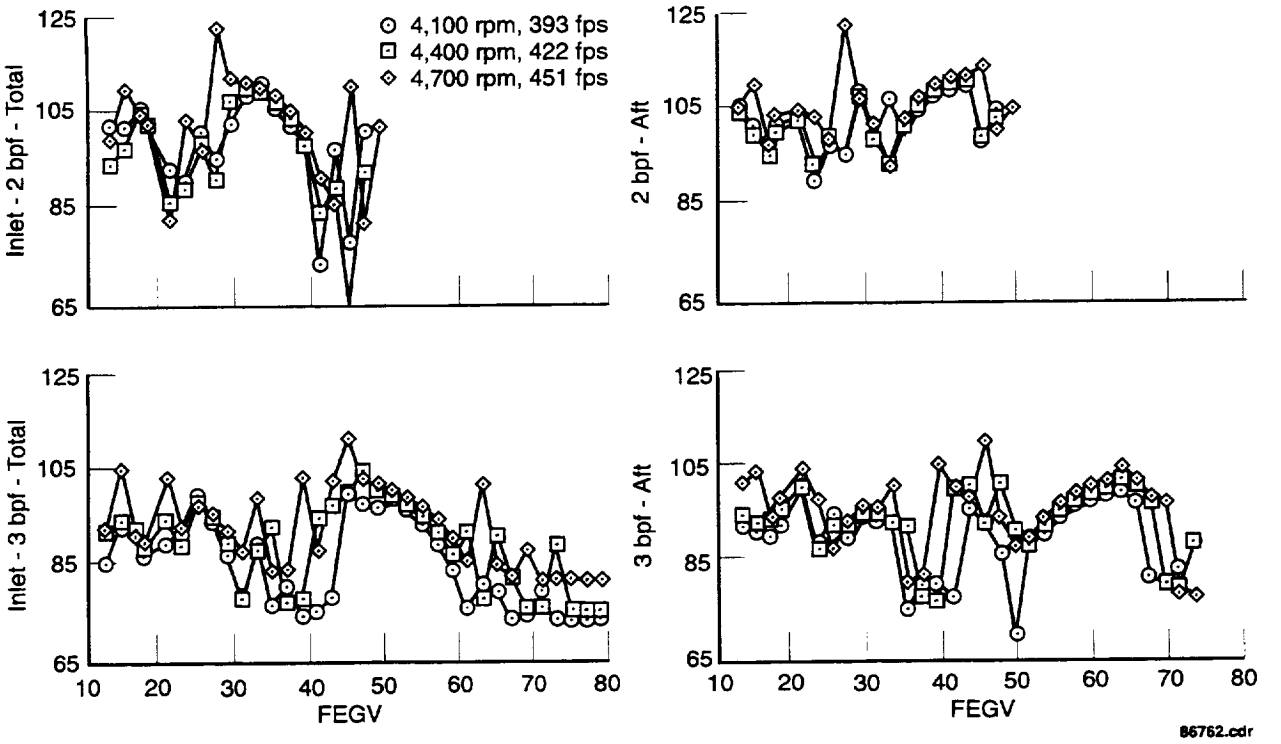

Figure 23. Predicted Tone Power Level for Fan 2 Versus Vane Number — Approach

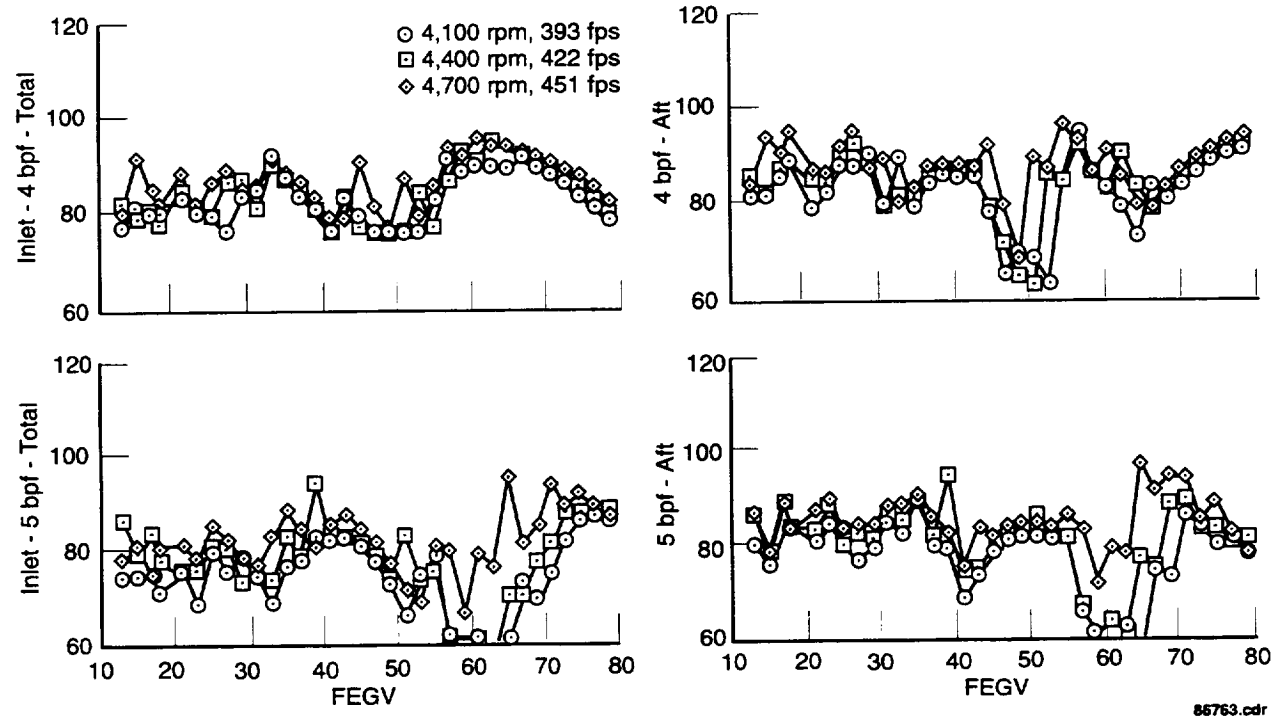

Figure 24. Predicted Tone Power Level for Fan 2 Versus Vane Number — Approach

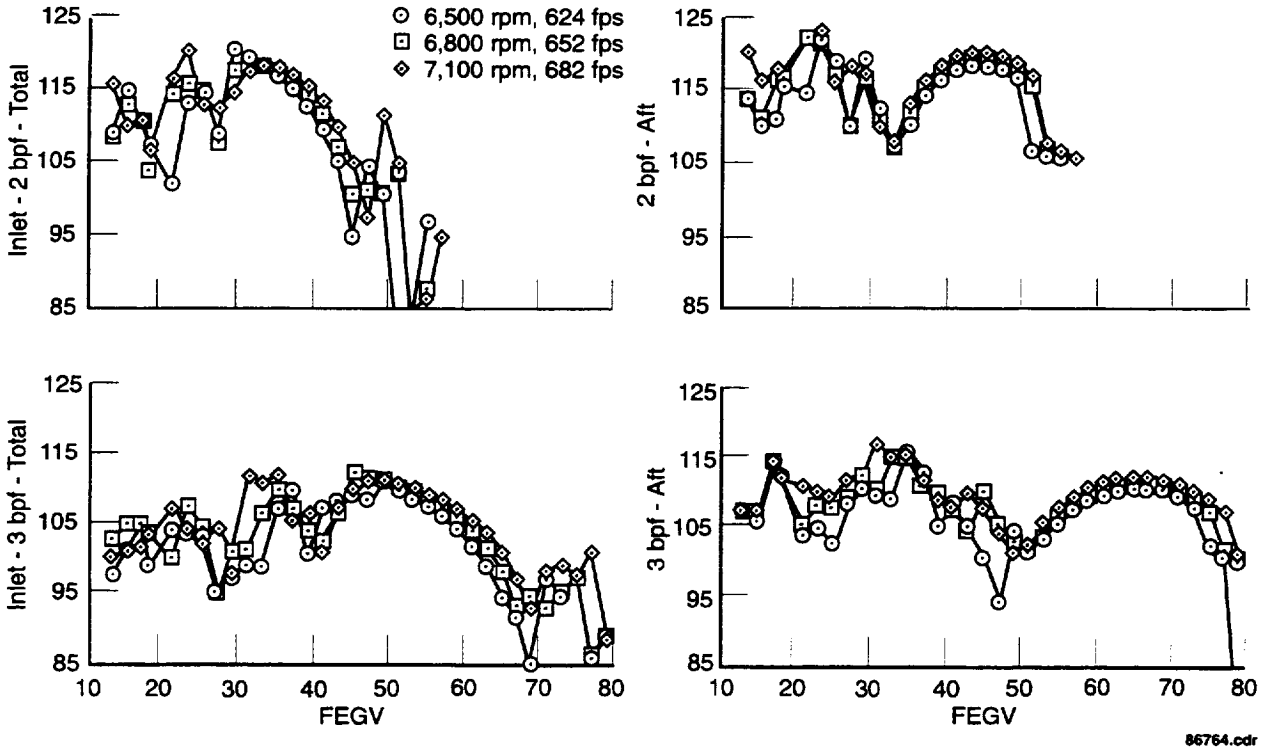

Figure 25. Predicted Tone Power Level for Fan 2 Versus Vane Number — Cutback

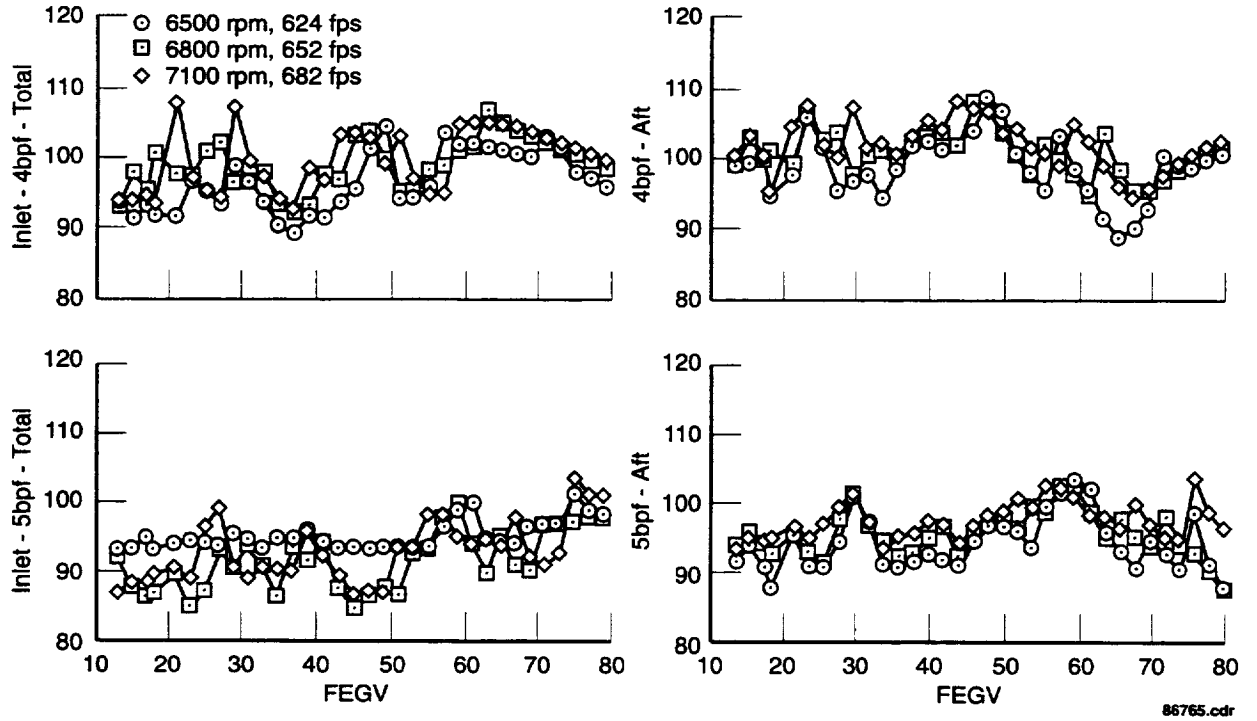

Figure 26. Predicted Tone Power Level for Fan 2 Versus Vane Number — Cutback

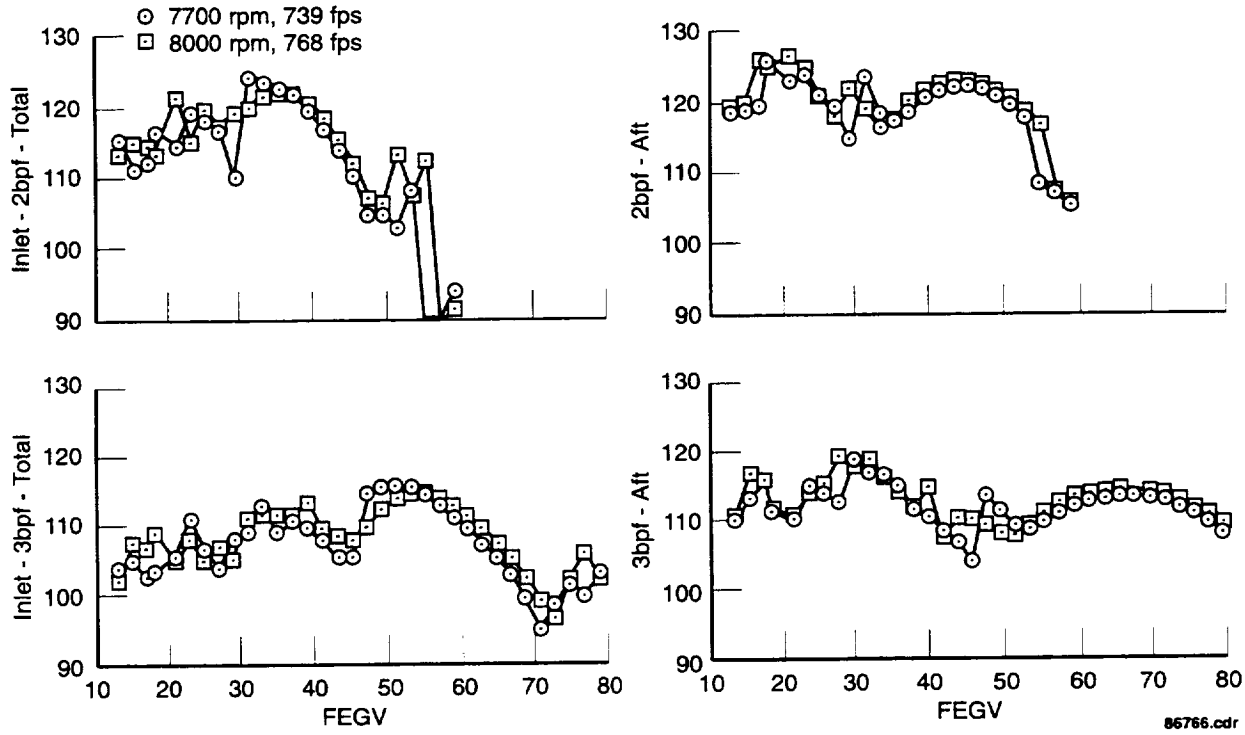

Figure 27. Predicted Tone Power Level for Fan 2 Versus Vane Number — SLTO

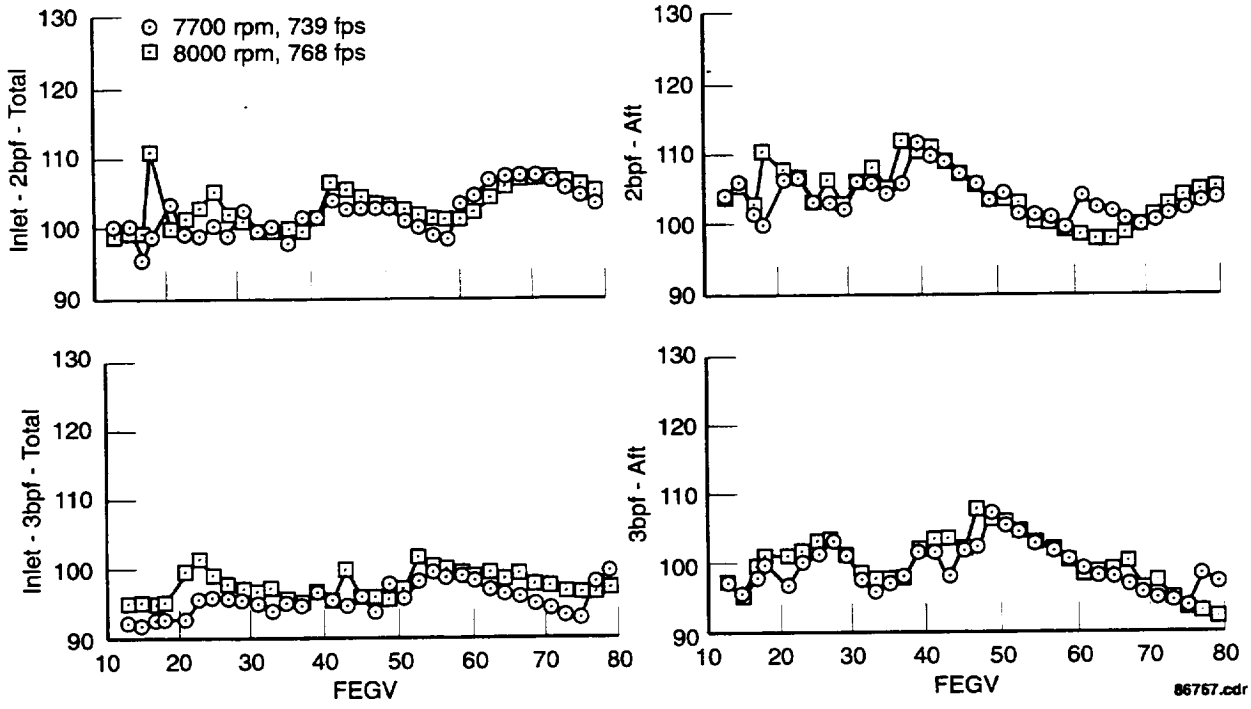

Figure 28. Predicted Tone Power Level for Fan 2 Versus Vane Number — SLTO

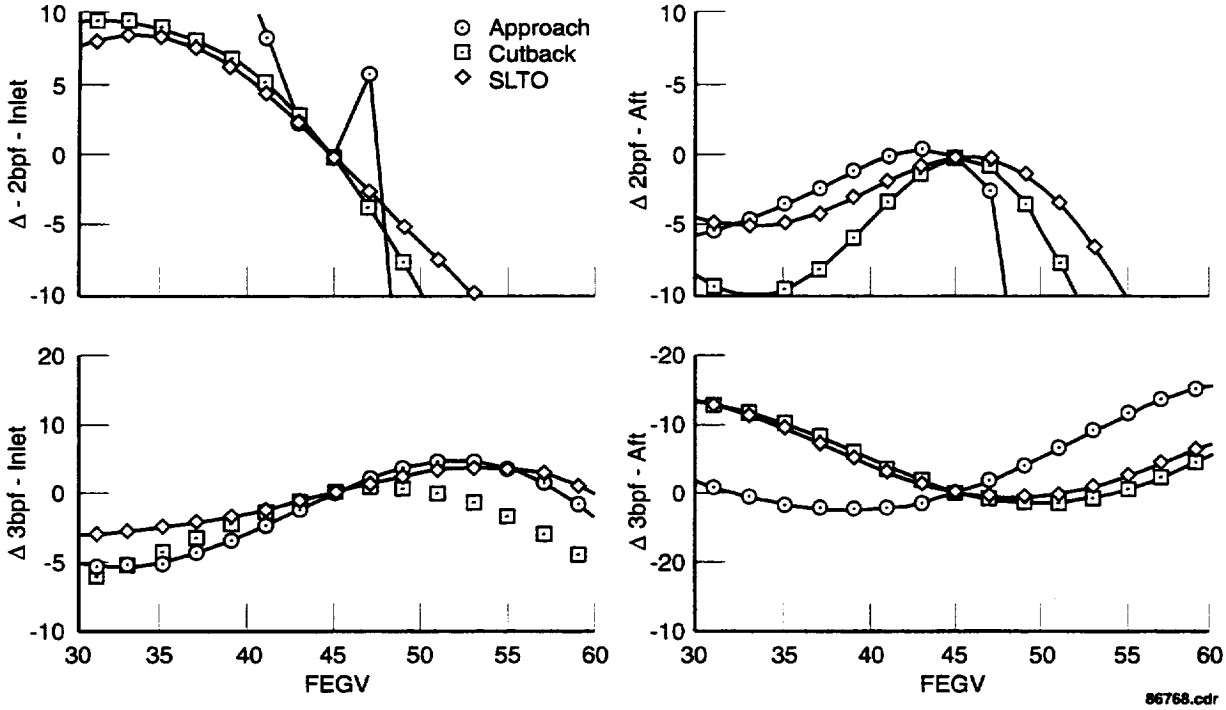

Figure 29. Tone Power-Level Δ Reference to Vane = 45 Approach, Cutback, and SLTO

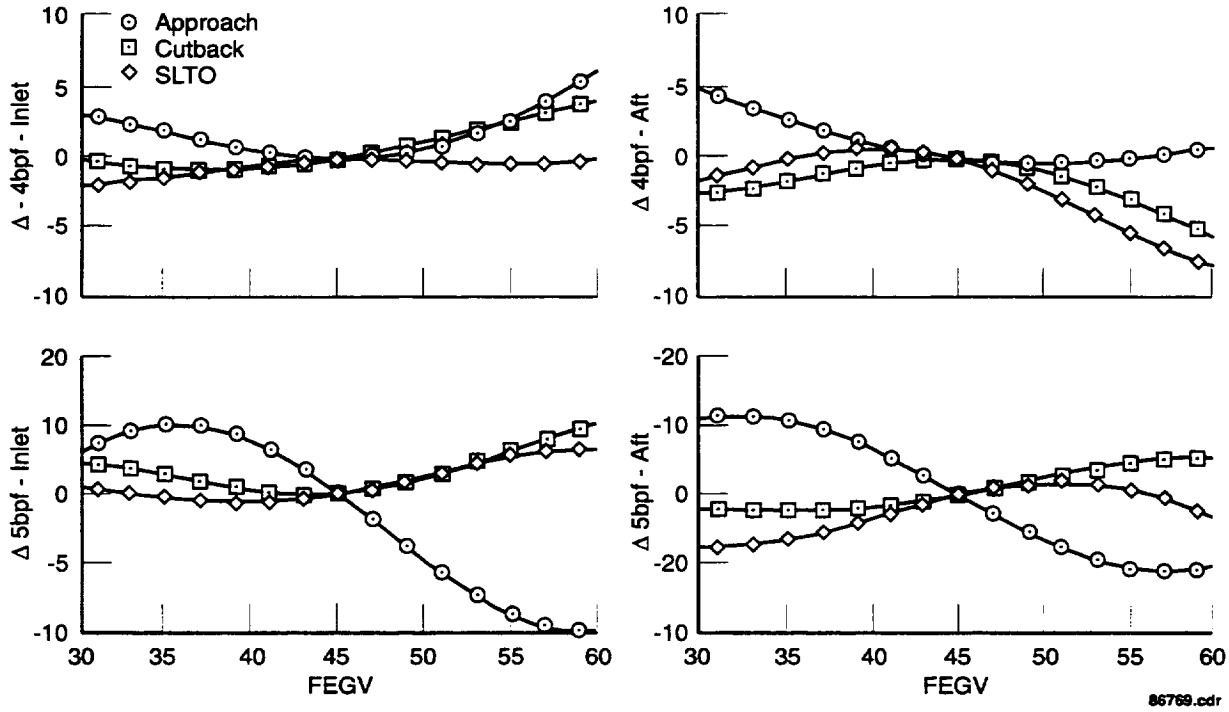

Figure 30. Tone Power-Level Δ Reference to Vane = 45 Approach, Cutback, and SLTO

For vane number > 45 —

- 2bpf is reduced at all three conditions
- 3bpf increases then decreases in the inlet and aft
- 4bpf increases in the inlet
- 4bpf decreases at cutback and SLTO in the aft
- 4bpf and 5bpf levels are generally 10 dB lower then 2bpf and 3bpf as observed from Figures 23, 24, 25, 26, 27, and 28.

Special one-third octave band fan-tone-only files were created with Δs from the curve fit data shown in Figures 29 and 30 so tone levels relative to vane = 45 could be read and then edited into the proper frequency location in the file. All frequencies not containing fan-tones were set to zero. The tone Δ files were then arithmetically added to the vane = 45 file to produce a set of tone level matrices for each vane number. Each fan-tone file was then logarithmically added to the broadband noise level that was previously source separated and defined from the vane = 45 Fan 1 data set, to create new fan noise spectra for each vane number. This was done at each of the three conditions of approach, cutback, and SLTO.

A series of examples are shown in one-third octave band spectra. Each figure shows the vane = 45 spectrum and a newly created spectrum consistent with the fan-tone Δs for vane = 51 applied and recombined with the broadband (Figures 31 through 35). By studying the figures, it can be seen how the predicted fan-tone Δ, applied to the measured data, altered the spectra.

4.5 CALCULATION OF SIMULATED FLIGHT PREDICTIONS

A calculation was performed that provided a single number metric for a simulated flyover. The spectra as described in Section 4.4 consisted of model data that had been scaled and extrapolated to a full-scale engine size and a uniform radius. Fan-tone Δs were applied to each spectrum to shape the spectrum for each vane number at the conditions of approach, cutback, and SLTO. Matrices of these spectra consisted of 32 angles, from 24 to 130 deg off the forward centerline.

The approach matrices were then extrapolated to an altitude of 121.9m (400 ft) and the cutback and SLTO matrices were extrapolated to an altitude of 457.2m (1500 ft). Atmospheric absorption was included over the extrapolated distances at FAA standard day conditions of 77°F and 70 percent relative humidity. An integration routine calculated a PNLTi for each matrix and included a *weighting* to simulate the contribution of the different angles, inlet to aft, during a flyover event. This simulated flyover metric was called an integrated PNLTi. A PNLTi was calculated for each odd vane number from 31 to 61 at each of the conditions of approach, cutback and SLTO. Thirty-one was the lowest vane number calculated because below this number bpf would be cut on for the approach condition. A cut on bpf was considered unacceptable. Sixty-one was the highest vane number calculated because structural considerations with the smaller chord became unacceptable. The PNLTi was the metric to be optimized to select the vane number for the Fan 2 stage design.

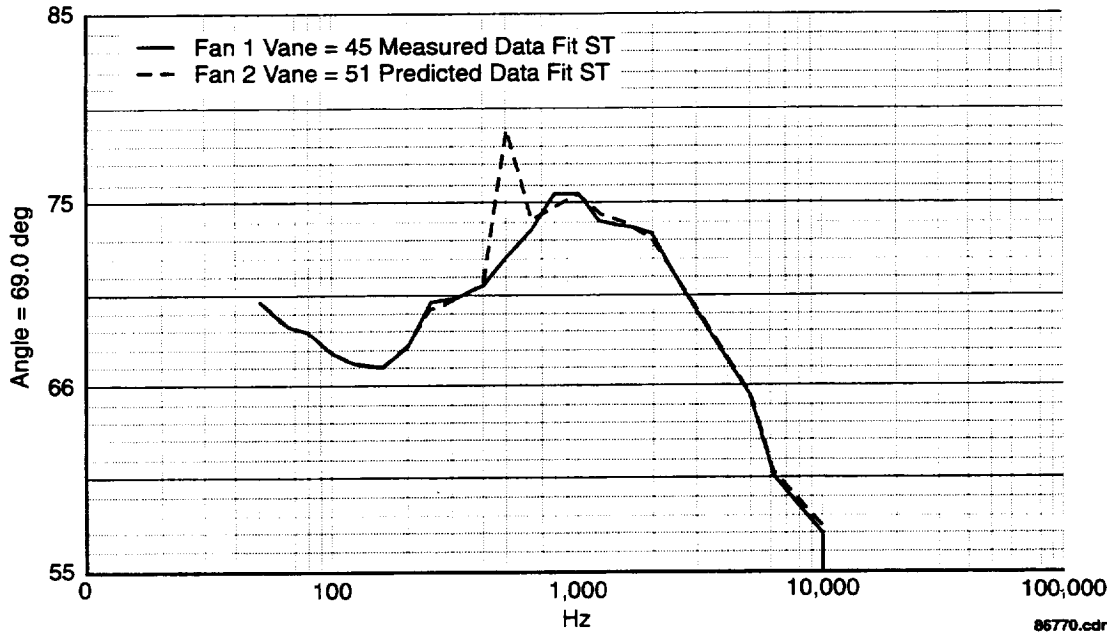

Figure 31. Fan 1 Vane = 45 Measured Spectra and Fan 2 Vane = 51, 69-deg Predicted Approach Condition Inlet Angle

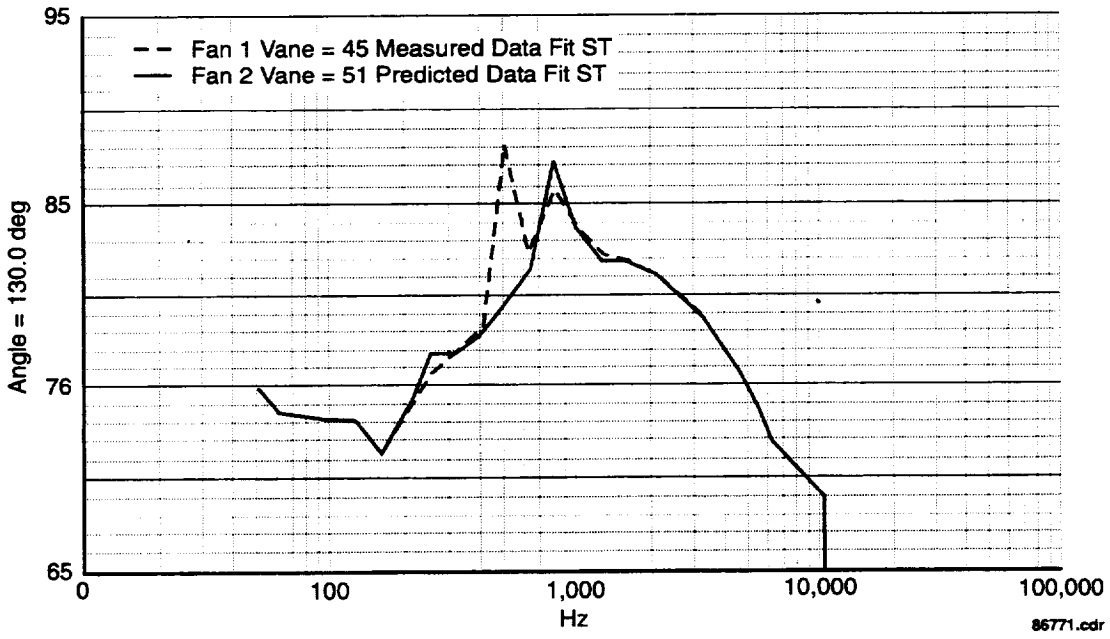

Figure 32. Fan 1 Vane = 45 Measured Spectra and Fan 2 Vane = 51, 130-deg Predicted Approach Condition Aft Angle

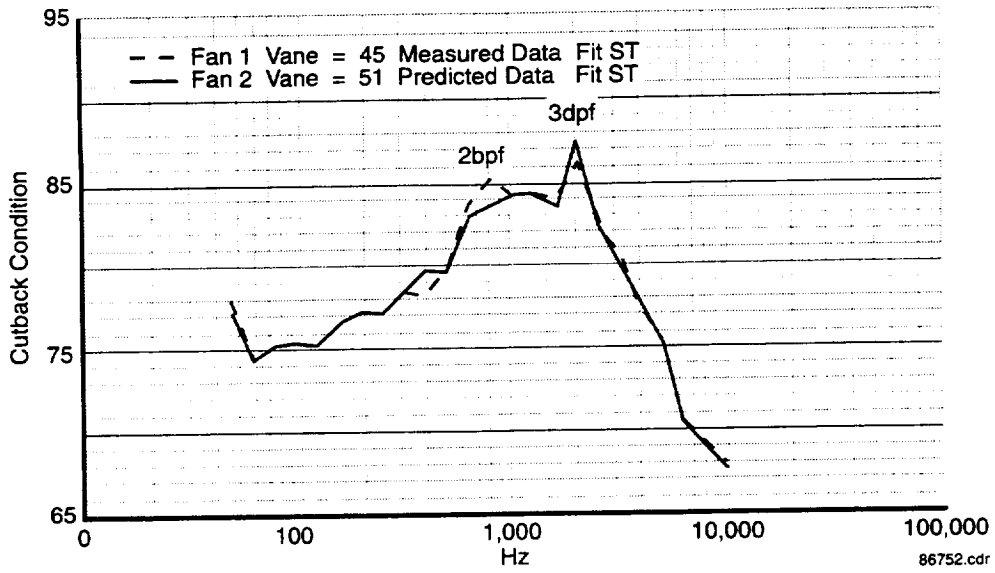

Figure 33. Fan 1 Vane = 45 Measured Spectra and Fan 2 Vane = 51, 69-deg Predicted Cutback Condition Inlet Angle

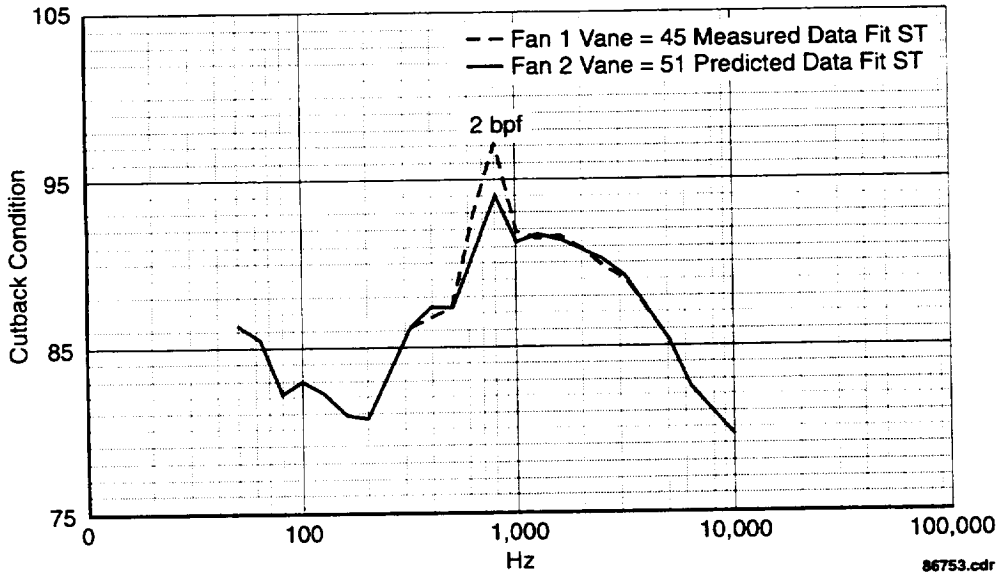

Figure 34. Fan 1 Vane = 45 Measured Spectra and Fan 2 Vane = 51 130-deg Predicted Cutback Condition Inlet Angle

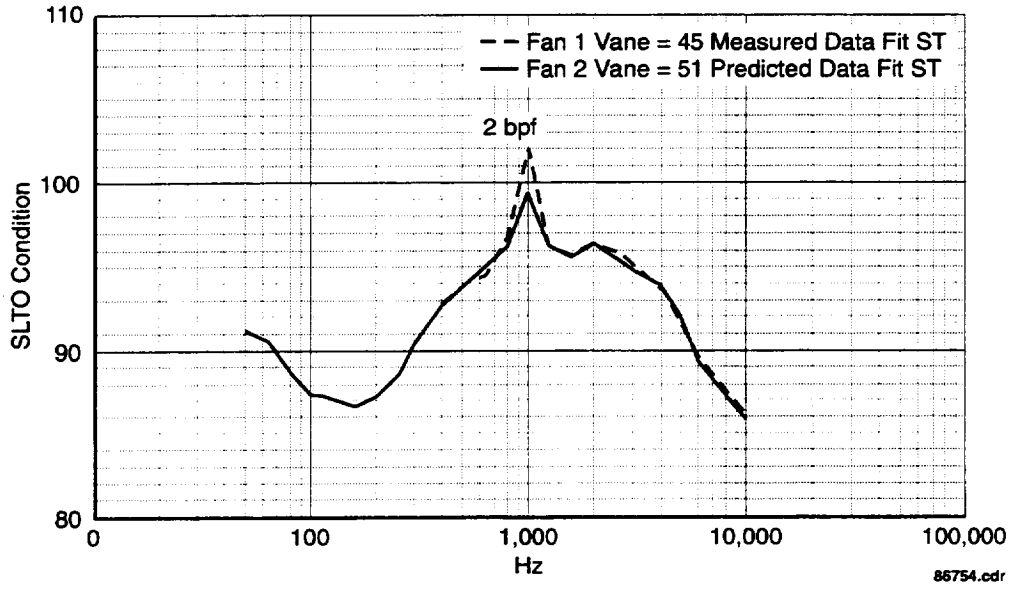

Figure 35. Fan 1 Vane = 45 Measured Spectra and Fan 2 Vane = 51, 130-deg Predicted SLTO Condition Inlet Angle

4.6 OPTIMIZATION OF NUMBER OF FEGVS

Observations from Sections 4.2 and 4.3 (predicted Fan 2 tone power levels and measured Fan 1 data) indicated a vane number that reduced 2bpf would be beneficial. However, a simple optimization of reducing 2bpf would ignore the contributions of other fan tones, including frequency weighting, to the overall noise. Therefore the PNLTi was selected as the metric to optimize based on discussions in Section 4.5.

Fan 1 stage had 18 blades and 45 vanes. It was assumed for the purpose of optimizing the vane number for the new fan stage, the Fan 2 stage design of 18 blades and 45 vanes would be used to represent the baseline fan stage design. It was noted in Section 4.3 how the predicted tone power-level trends were similar for Fan 1 and Fan 2 as a function of vane number, even though Fan 2 is designed for 10 percent lower operating speeds. Therefore Δs relative to 45 vanes were calculated to optimize the vane number. The calculated PNLTi for the Fan 2 stage of 18 blades and 45 vanes was subtracted from the calculated PNLTi for each vane number and at each of the three conditions of approach, cutback, and SLTO. Therefore, a negative Δ represented lower noise.

One vane number could provide lower noise at one condition, i.e., approach, but increased noise at one or both of the other conditions. Figure 36 illustrates the results of these calculated Δs at each of the three conditions. Note that for the approach condition, there is a significant noise increase below a vane count of 45. (Referring to Figures 23 and 24, one can see this was due to the increasing levels of 2bpf.) One can also observe the Δ for the approach condition at vane = 53 was optimum, but the SLTO Δ was minimal. Increasing the vane count beyond 53 shows the approach Δ vanishing and the SLTO Δ maximizing and the cutback Δ decreases to zero slowly, then becomes positive beyond 58. Below 49, the approach Δ rises dramatically.

This study then assumed noise at each of the three conditions was equally important. Therefore, a cumulative PNLTi Δ was calculated and plotted for all three conditions. The cumulative Δ at all three conditions is shown in Figure 37. The plot indicated the maximum noise benefit due to a change in vane count was either 51 or 53 and was equal to 1.1 cumulative EPNdB at the three conditions.

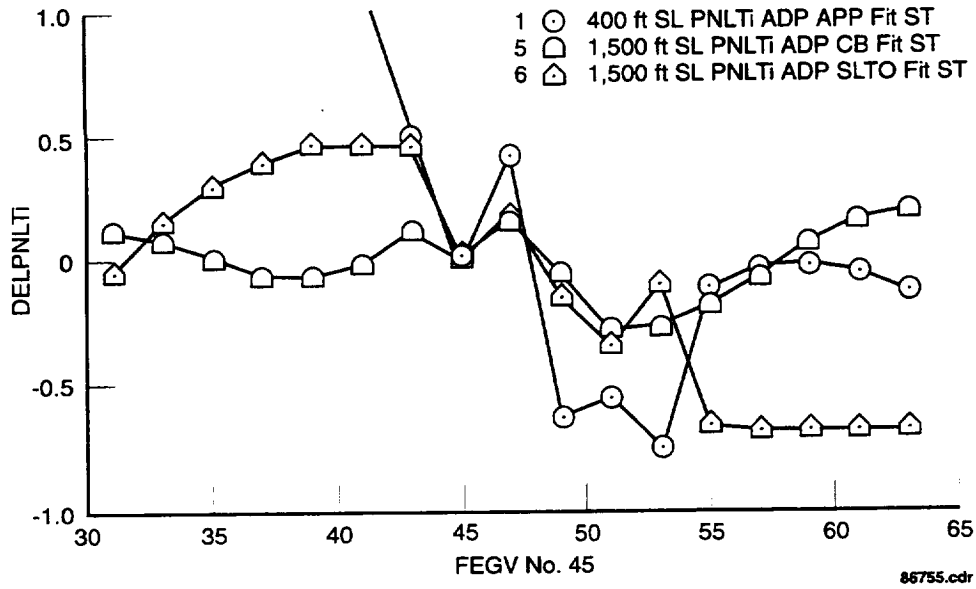

Figure 36. Noise Δ (PNLTi) Relative to Vane = 45 at Approach, Cutback, and Sideline

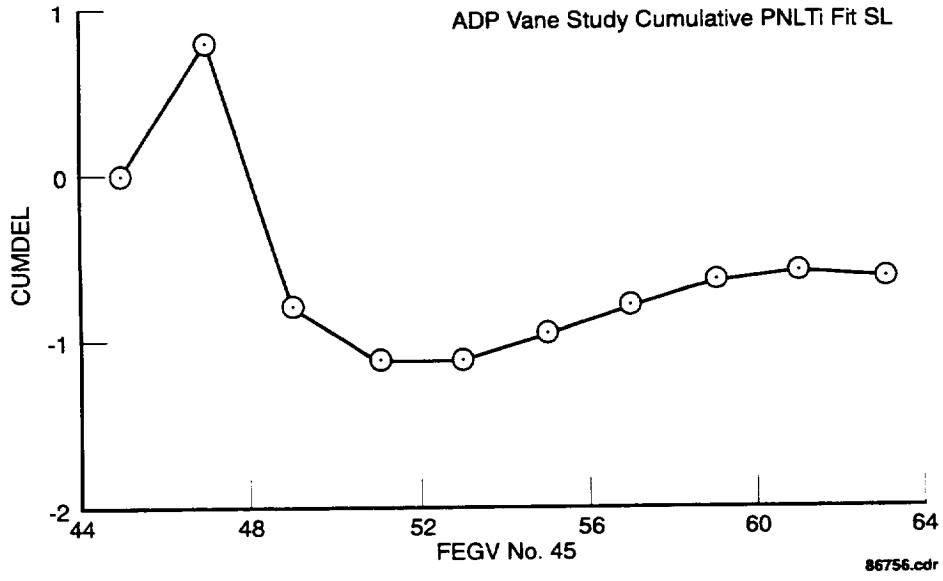

Figure 37. Noise Δ (PNLTi) Relative to Vane = 45 Cumulative at Approach, Cutback, and Sideline

A comparison of the predicted fan-tone power levels for 2bpf through 5bpf for the nominal baseline of vane = 45 and vane = 51 is shown as a function of fan tip speed in Figures 38 and 39. In almost every instance, the vane count of 51 provides equal or lower tone power levels than 45 vanes. This is particularly evident in the case of aft radiated 2bpf. There are noted exceptions for 3bpf and 5bpf at fan tip speeds near the cutback condition.

The question of what the maximum noise reduction would be if all the tones could be completely eliminated still remained. The broadband-only (fan tones removed) spectra for the vane = 45 case was used to calculate an effective perceived noise level (PNL) and this was assumed to remain constant over the range of vanes = 31 through 61. This level was compared to the total PNLTi as described in Section 4.5 to see what the maximum reduction in noise would be if no tones were present in the spectra. This was done for the three flight conditions and the results are shown in Figures 40, 41, and 42. The maximum reduction in total noise was 2.1, 0.9, and 0.9 EPNdB for three conditions with vane = 45. (Cumulative benefit = 3.9 EPNdB.) The vane = 51 case reduced total noise relative to vane = 45, by 0.5, 0.3 and 0.3 EPNdB, achieving a 1.1 EPNdB cumulative reduction relative to the maximum reduction of 3.9 EPNdB by eliminating all fan tones from the spectra.

4.7 ESTIMATE OF TOTAL NOISE REDUCTION OF FAN 2

Fan 1 data were acquired and provided a benchmark against which Fan 2 data could be compared when its noise is measured. An estimate of the reduction in noise from Fan 1 to Fan 2 was made by summing the following Δs. The Δ noise unit is a simulated flyover noise level in EPNL. A subjective review of Fan 1 and Fan 2 predicted wakes was made. With no calibration of wake profile or depth to noise, no attempt was made to include this effect in the estimate.

Table 14. Fan Noise Comparison

Fan Noise Δ	*SLTO*	*Cutback*	*Approach*	*Cumulative*
-10% Tip Speed	-2.3	-2.3	-2.3	
Optimum Vane Number For Fan Tones	-0.5	-0.3	-0.3	
Increase in Vane Number for Broadband	0.3	0.3	0.3	
Total	-2.5	-2.3	-2.3	-7.1

4.8 RECOMMENDATION AND CONCLUSION

The optimum vane number to reduce noise by fan tone reduction was found to be 51. After consultation with the aero and structural designers of the fan stage, 51 was deemed acceptable for the 22 in. ADP model and future product application. Therefore, the final recommendation for optimum acoustic vane number was 51. The expected reduction in fan noise relative to Fan 1 is 7.1 EPNdB cumulative at three flight conditions.

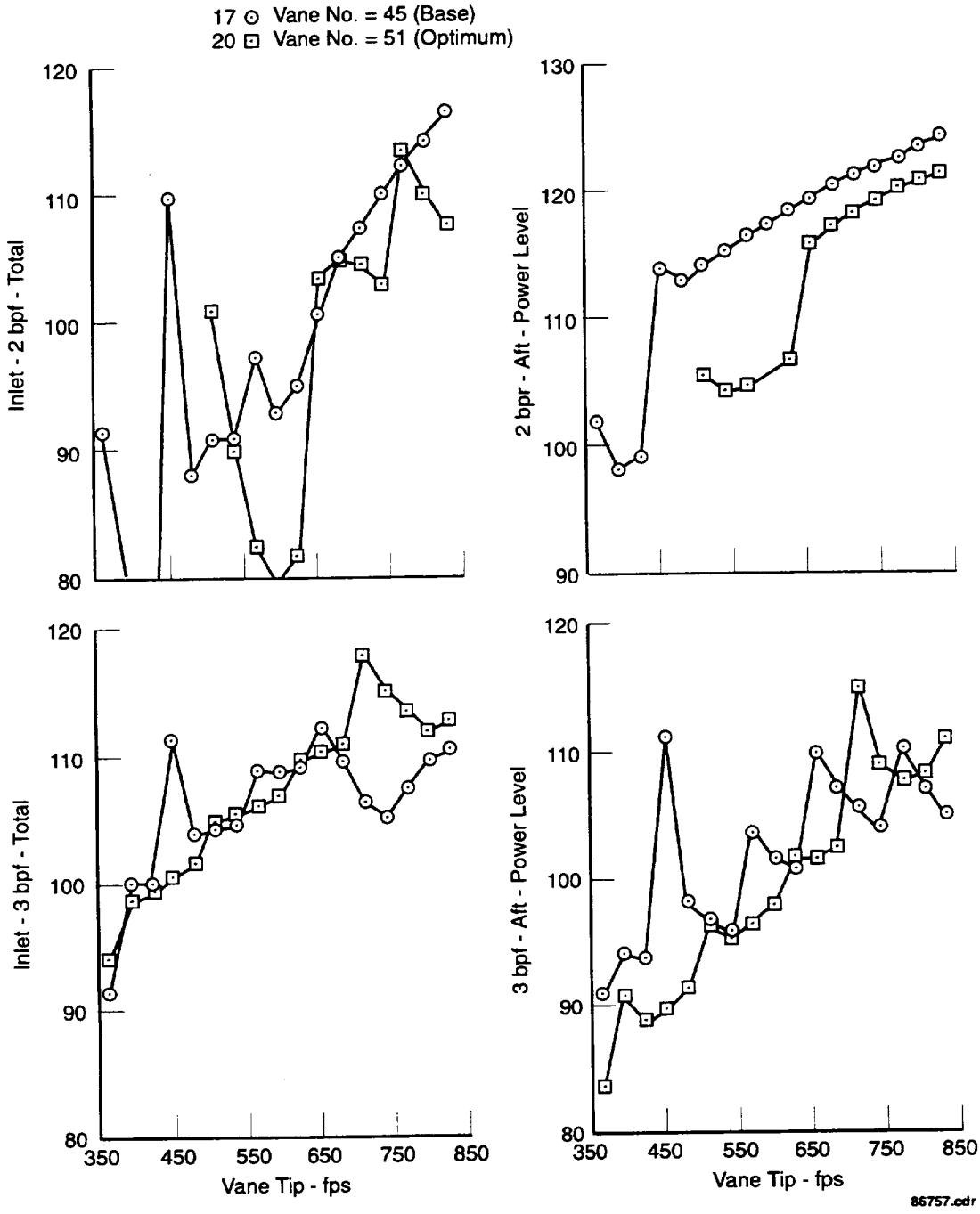

Figure 38. Predicted Fan-Tone Power Level Versus Fan Tip Speed Vane = 45 (Base) and 51 (Optimum)

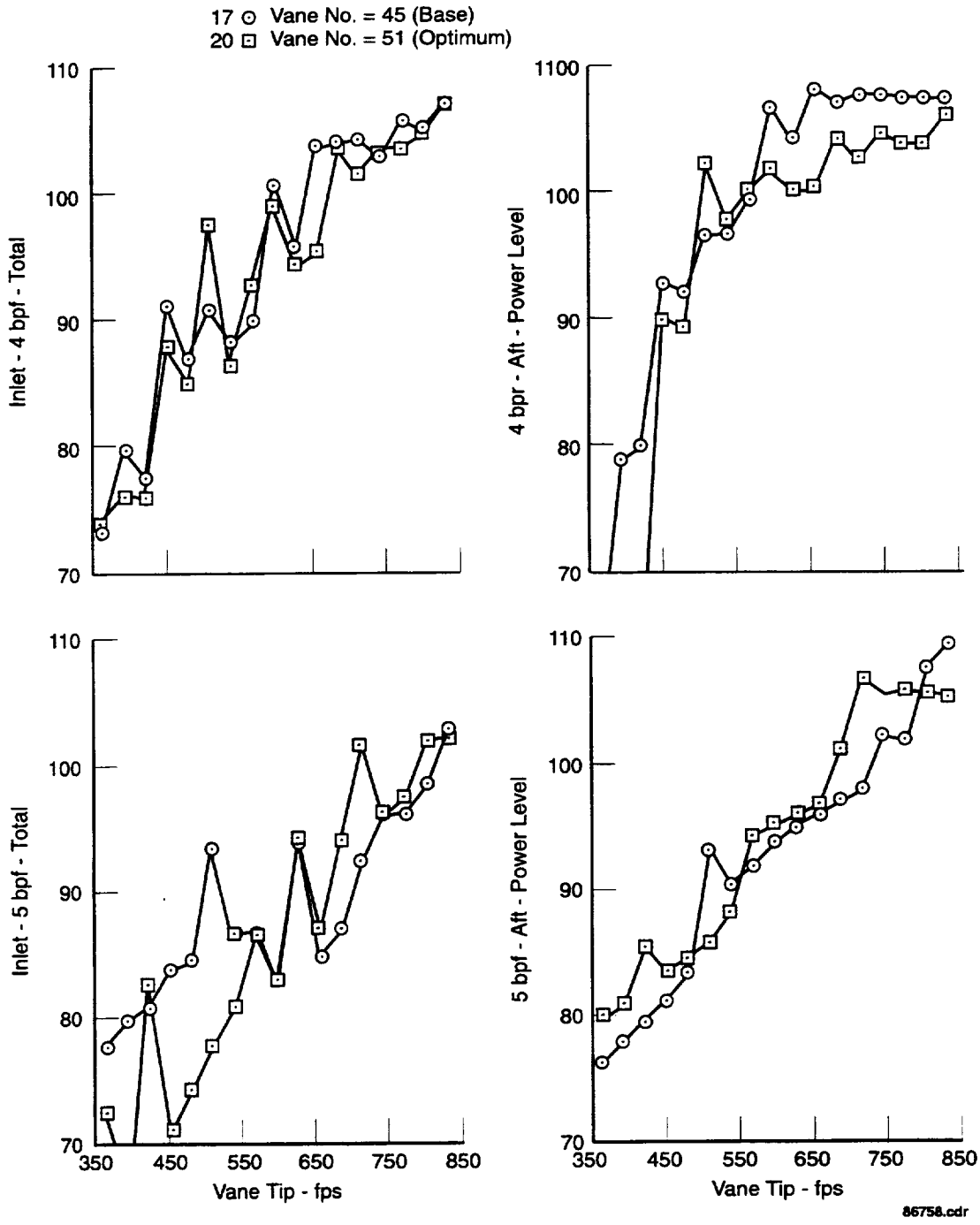

Figure 39. Predicted Fan-Tone Power Level Versus Fan Tip Speed Vane = 45 (Base) and 51 (Optimum)

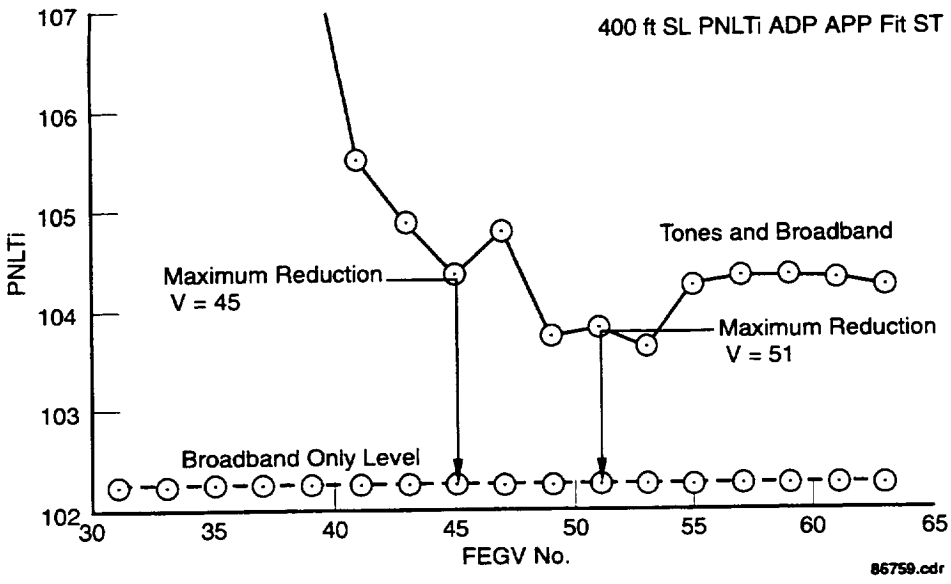

Figure 40. Maximum Noise Reduction Achievable at Approach by Eliminating All Tones

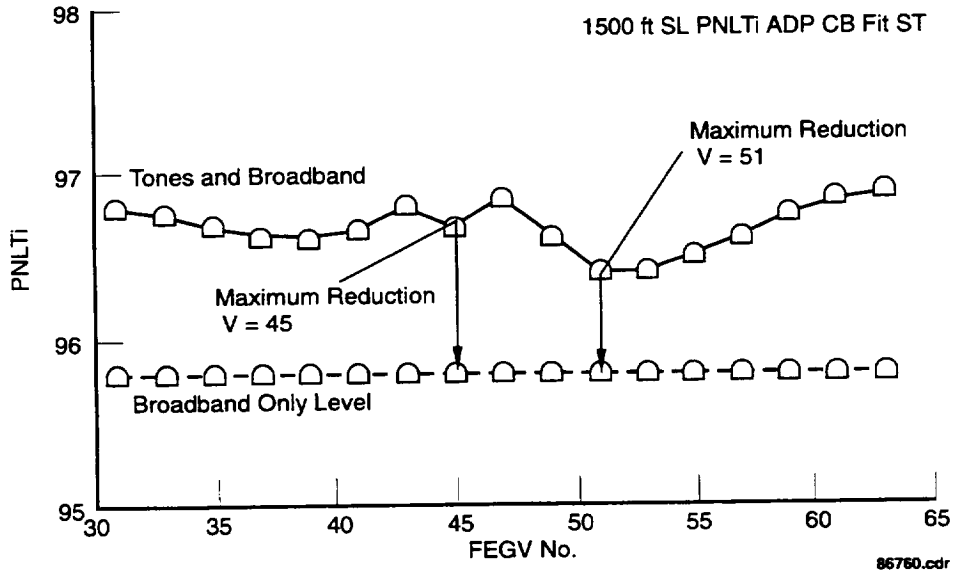

Figure 41. Maximum Noise Reduction Achievable at Cutback by Eliminating All Tones

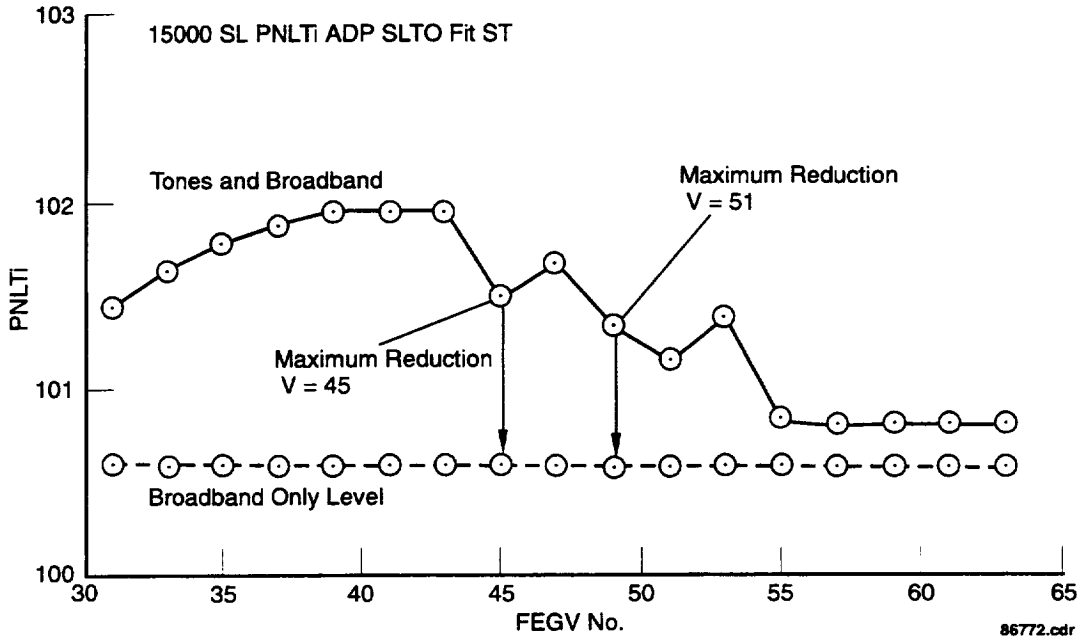

Figure 42. Maximum Noise Reduction Achievable at SLTO by Eliminating All Tones

5. CONCLUSIONS

This report described the aerodynamic, acoustic, and structural design of the Advanced Low-Noise Research Fan Stage. Based on the design and analysis presented in each of these areas, the model is expected to meet all design requirements. Testing of this model will provide essential information on the validity of the design assumptions and methods.

APPENDIX A — DESIGN VELOCITY VECTOR LISTING

Table A-1. Definition of Parameters

Symbol	*Definition*
-1	Condition at the airfoil leading edge
-2	Condition at the airfoil trailing edge
SL	Streamline number
V	Velocity
VM	Meridional velocity
Vθ	Tangential velocity
U	Tangential velocity of rotor blade
EPSI	Cone angle of the flow (PHI)
B	Air angle measured from axial (BETA)
M	Mach number
TURN	Turning angle (B′ minus B′-2*)
PCT TE SPAN	Percent span at trailing edge measured from hub to tip
N_{CORR} INLET	Corrected rotor angular velocity [viz, actual rpm divided by the square root of upstream total temperature over 288.2K (518.7R)]
W_{CORR} INLET	Corrected flow [actual mass flow multiplied by the square root of upstream total temperature over 288.2K (518.7R) and divided by the upstream total pressure over 10332 kg/m^2 (2116lb_f/ft^2)]

* Prime symbols indicate a quantity in the rotating frame, non-prime symbols indicate the stationary frame.

TABLE A-2. FAN BLADE

DESIGN POINT ROTOR

SL	V-1 m/sec	V-2 m/sec	VM-1 m/sec	VM-2 m/sec	V0-1 m/sec	V0-2 m/sec	U-1 m/sec	U-2 m/sec	V'-1 m/sec	V'-2 m/sec	V0'-1 m/sec	V0'-2 m/sec	EPSI-1 radian	EPSI-2 radian
1	219.0	220.0	219.0	200.2	0.0	91.3	100.6	106.2	241.0	200.7	-100.6	-14.9	0.0990	0.0531
2	216.9	223.6	216.9	197.7	0.0	104.5	106.9	112.2	241.8	197.8	-106.9	-7.7	0.1158	0.0463
3	215.9	227.5	215.9	195.2	0.0	116.9	113.3	118.2	243.8	195.2	-113.3	-1.3	0.1235	0.0441
4	214.6	233.9	214.6	189.5	0.0	137.1	132.3	136.3	252.1	189.5	-132.3	0.8	0.1243	0.0475
5	212.7	240.3	212.7	187.5	0.0	150.2	157.7	160.4	264.8	187.8	-157.7	-10.2	0.1066	0.0493
6	211.0	241.5	211.0	188.6	0.0	150.8	170.4	172.4	271.2	189.8	-170.4	-21.6	0.0935	0.0452
7	208.6	241.7	208.6	190.5	0.0	148.6	183.0	184.5	277.5	193.9	-183.0	-35.9	0.0792	0.0371
8	205.5	238.4	205.5	192.9	0.0	140.2	195.7	196.5	283.8	200.9	-195.7	-56.3	0.0649	0.0240
9	203.9	234.2	203.9	193.1	0.0	132.5	202.1	202.5	287.1	205.4	-202.1	-70.1	0.0579	0.0143
10	202.6	227.1	202.6	189.9	0.0	124.6	208.4	208.6	290.7	207.6	-208.4	-84.0	0.0531	0.0025
11	202.2	218.0	202.2	181.3	0.0	121.1	214.8	214.6	295.0	203.9	-214.8	-93.5	0.0522	-0.0140

SL	B-1 degree	B-2 degree	B'-1 degree	B'-2 degree	M-1	M-2	M'-1	M'-2	TURN degree
1	0.0	24.4	24.65	4.24	0.6718	0.6633	0.7393	0.6052	20.41
2	0.0	27.8	26.29	2.23	0.6648	0.6725	0.7412	0.5951	24.06
3	0.0	30.9	27.78	0.38	0.6614	0.6828	0.7469	0.5857	27.40
4	0.0	35.9	31.80	-0.25	0.6571	0.6978	0.7720	0.5652	32.05
5	0.0	38.7	36.68	3.11	0.6509	0.7119	0.8102	0.5564	33.57
6	**0.0**	**38.7**	**39.02**	**6.54**	**0.6453**	**0.7134**	**0.8293**	**0.5607**	**32.49**
7	0.0	38.0	41.34	10.66	0.6374	0.7123	0.8479	0.5715	30.68
8	0.0	36.0	43.66	16.29	0.6271	0.7017	0.8660	0.5913	27.37
9	0.0	34.5	44.79	19.94	0.6218	0.6889	0.8754	0.6043	24.85
10	0.0	33.3	45.85	23.85	0.6175	0.6671	0.8859	0.6098	22.00
11	0.0	33.8	46.76	27.28	0.6163	0.6382	0.8990	0.5970	19.48

SL	V-1 ft/sec	V-2 ft/sec	VM-1 ft/sec	VM-2 ft/sec	V0-1 ft/sec	V0-2 ft/sec	U-1 ft/sec	U-2 ft/sec	V'-1 ft/sec	V'-2 ft/sec	V0'-1 ft/sec	V0'-2 ft/sec	EPSI-1 degree	EPSI-2 degree	PCT TE span
1	718.5	721.9	718.5	656.8	0.0	299.5	330.1	348.4	790.7	658.6	-330.1	-49.0	5.674	3.041	0.0500
2	711.6	733.6	711.6	648.6	0.0	342.8	350.9	368.2	793.4	649.1	-350.9	-25.4	6.635	2.654	0.1000
3	708.2	746.5	708.2	640.3	0.0	383.7	371.7	387.9	799.8	640.3	-371.7	-4.3	7.077	2.527	0.1500
4	704.1	767.4	704.1	621.7	0.0	450.0	434.1	447.2	827.1	621.7	-434.1	2.8	7.119	2.722	0.3000
5	697.9	788.3	697.9	615.3	0.0	492.8	517.3	526.2	868.7	616.2	-517.3	-33.4	6.108	2.825	0.5000
6	692.3	792.3	692.3	618.7	0.0	494.9	559.0	565.8	889.8	622.7	-559.0	-70.9	5.356	2.589	0.6000
7	684.5	792.9	684.5	625.2	0.0	487.6	600.6	605.3	910.6	636.1	-600.6	-117.6	4.539	2.126	0.7000
8	674.3	782.3	674.3	632.8	0.0	460.0	642.2	644.8	931.2	659.3	-642.2	-184.8	3.719	1.377	0.8000
9	669.0	768.4	669.0	633.6	0.0	434.7	663.0	664.5	941.9	674.0	-663.0	-229.8	3.316	0.818	0.8500
10	664.7	745.2	664.7	623.0	0.0	408.9	683.8	684.3	953.6	681.2	-683.8	-275.4	3.043	0.143	0.9000
11	663.5	715.3	663.5	594.7	0.0	397.4	704.6	704.1	967.8	669.1	-704.6	-306.6	2.992	-0.803	0.9500

Ncorr inlet rpm	Wcorr inlet lbm/sec	Wcorr inlet kg/sec	PO/PO inlet
7556.80	91.8190	41.6488	1.2877

TABLE A-3. FAN EXIT GUIDE VANE

DESIGN POINT FECV

SL	V-1 m/sec	V-2 m/sec	VM-1 m/sec	VM-2 m/sec	VO-1 m/sec	VO-2 m/sec	EPSI-1 radian	EPSI-2 radian
1	169.9	141.4	128.7	141.4	111.0	0.0	0.1572	0.2282
2	182.5	148.4	140.1	148.4	116.9	0.0	0.1731	0.2148
3	192.6	154.6	149.4	154.6	121.6	0.0	0.1790	0.2016
4	214.5	170.1	167.6	170.1	133.9	0.0	0.1679	0.1612
5	231.8	186.4	181.8	186.4	143.8	0.0	0.1223	0.1042
6	235.0	192.7	185.5	192.7	144.3	0.0	0.0952	0.0752
7	233.3	196.4	186.1	196.4	140.7	0.0	0.0675	0.0459
8	224.7	194.2	182.2	194.2	131.4	0.0	0.0419	0.0178
9	215.5	188.5	175.9	188.5	124.5	0.0	0.0305	0.0042
10	203.0	179.8	164.3	179.8	119.1	0.0	0.0195	-0.0103
11	186.6	167.9	145.4	167.9	117.0	0.0	0.0070	-0.0284

SL	B-1 degree	B-2 degree	M-1	M-2	TURN degree
1	39.8	0.0	0.5001	0.4128	39.82
2	39.1	0.0	0.5378	0.4331	39.11
3	38.6	0.0	0.5683	0.4510	38.61
4	38.4	0.0	0.6334	0.4948	38.39
5	**38.3**	**0.0**	**0.6833**	**0.5408**	**38.31**
6	37.9	0.0	0.6917	0.5585	37.87
7	37.1	0.0	0.6852	0.5691	37.10
8	35.8	0.0	0.6580	0.5626	35.83
9	35.3	0.0	0.6298	0.5459	35.29
10	35.9	0.0	0.5910	0.5198	35.93
11	38.8	0.0	0.5403	0.4835	38.79

SL	V-1 ft/sec	V-2 ft/sec	VM-1 ft/sec	VM-2 ft/sec	VO-1 ft/sec	VO-2 ft/sec	PCT TE span	EPSI-1 degree	EPSI-2 degree
1	557.6	463.8	422.2	463.8	364.1	0.0	0.0500	9.007	13.078
2	598.8	487.0	459.8	487.0	383.5	0.0	0.1000	9.915	12.306
3	632.0	507.4	490.1	507.4	399.1	0.0	0.1500	10.255	11.551
4	703.8	557.9	549.9	557.9	439.2	0.0	0.3000	9.619	9.236
5	760.4	611.7	596.3	611.7	471.8	0.0	0.5000	7.005	5.971
6	771.0	632.1	608.6	632.1	473.3	0.0	0.6000	5.454	4.309
7	765.4	644.3	610.6	644.3	461.5	0.0	0.7000	3.868	2.632
8	737.1	637.2	597.8	637.2	431.2	0.0	0.8000	2.399	1.019
9	707.1	618.5	577.2	618.5	408.4	0.0	0.8500	1.746	0.238
10	665.9	590.1	539.2	590.1	390.8	0.0	0.9000	1.119	-0.591
11	612.2	550.9	477.0	550.9	383.8	0.0	0.9500	0.403	-1.630

Ncorr inlet rpm	Wcorr inlet lbm/sec	Wcorr inlet kg/sec
7556.80	91.82	41.65

TABLE A-4 CORE STATOR

DESIGN POINT CORE STATOR

SL	V-1 m/sec	V-2 m/sec	VM-1 m/sec	VM-2 m/sec	VO-1 m/sec	VO-2 m/sec	EPSI-1 radian	EPSI-2 radian
1	168.8	133.5	144.7	133.5	87.0	0.0	-0.2353	-0.0183
2	171.1	137.0	146.6	137.0	88.3	0.0	-0.2282	-0.0211
3	173.4	140.5	148.5	140.5	89.6	0.0	-0.2212	-0.0240
4	180.5	151.0	154.3	151.0	93.6	0.0	-0.2058	-0.0318
5	190.1	164.5	162.2	164.5	99.2	0.0	-0.1978	-0.0406
6	194.9	170.7	166.0	170.7	102.1	0.0	-0.1976	-0.0443
7	199.5	176.8	169.6	176.8	105.0	0.0	-0.1992	-0.0479
8	204.0	182.7	173.1	182.7	107.9	0.0	-0.2023	-0.0511
9	206.6	185.6	175.3	185.6	109.4	0.0	-0.2257	-0.0527
10	209.7	188.7	178.0	188.7	110.9	0.0	-0.2730	-0.0542
11	212.7	191.7	180.6	191.7	112.3	0.0	-0.3202	-0.0557

SL	B-1 degree	B-2 degree	M-1	M-2	TURN degree
1	31.5	0.0	0.5015	0.3929	31.48
2	31.5	0.0	0.5086	0.4035	31.49
3	31.5	0.0	0.5156	0.4141	31.49
4	31.5	0.0	0.5373	0.4457	31.54
5	31.7	0.0	0.5668	0.4866	31.73
6	**31.9**	**0.0**	**0.5815**	**0.5055**	**31.85**
7	32.0	0.0	0.5957	0.5240	32.03
8	32.2	0.0	0.6095	0.5420	32.24
9	32.4	0.0	0.6177	0.5510	32.39
10	32.7	0.0	0.6273	0.5604	32.66
11	33.0	0.0	0.6369	0.5697	32.98

SL	V-1 ft/sec	V-2 ft/sec	VM-1 ft/sec	VM-2 ft/sec	VO-1 ft/sec	VO-2 ft/sec	PCT TE span	EPSI-1 degree	EPSI-2 degree
1	553.8	437.9	474.7	437.9	285.3	0.0	0.0500	-13.482	-1.050
2	561.4	449.5	481.0	449.5	289.6	0.0	0.1000	-13.077	-1.211
3	569.0	461.1	487.3	461.1	293.9	0.0	0.1500	-12.673	-1.372
4	592.2	495.5	506.4	495.5	307.1	0.0	0.3000	-11.790	-1.824
5	623.8	539.7	532.1	539.7	325.6	0.0	0.5000	-11.335	-2.324
6	639.5	560.1	544.7	560.1	334.9	0.0	0.6000	-11.320	-2.540
7	654.6	580.0	556.6	580.0	344.5	0.0	0.7000	-11.415	-2.742
8	669.2	599.3	567.9	599.3	354.1	0.0	0.8000	-11.589	-2.926
9	677.9	609.1	575.0	609.1	358.9	0.0	0.8500	-12.934	-3.017
10	687.9	619.0	583.9	619.0	363.7	0.0	0.9000	-15.640	-3.105
11	697.9	628.9	592.7	628.9	368.5	0.0	0.9500	-18.345	-3.194

Ncorr inlet rpm	Wcorr inlet lbm/sec	Wcorr inlet kg/sec
7556.80	91.82	41.65

APPENDIX B — FLOWPATH COORDINATES

Table B-1. Fan Outer Flowpath

AXIAL	RADIUS	
-12.75000	11.17150	
-12.74216	11.08857	
-12.71779	11.00376	
-12.67575	10.91779	
-12.61515	10.83151	
-12.53545	10.74584	
-12.43645	10.66178	
-12.31841	10.58034	
-12.18203	10.50253	
-12.02843	10.42933	
-11.85917	10.36163	
-11.67617	10.30019	
-11.48166	10.24563	
-11.27806	10.19842	
-11.06790	10.15882	
-10.85373	10.12694	
-10.63802	10.10270	
-10.42310	10.08588	
-10.21106	10.07613	
-10.00375	10.07300	
-9.72776	10.07508	
-9.45176	10.08131	
-9.17577	10.09164	
-8.89977	10.10596	
-8.62377	10.12416	
-8.34778	10.14608	
-8.07178	10.17151	
-7.79579	10.20025	
-7.51979	10.23202	
-7.24380	10.26655	
-6.96781	10.30354	
-6.69182	10.34266	
-6.41584	10.38357	
-6.13985	10.42589	
-5.86387	10.46926	
-5.58788	10.51330	
-5.31190	10.55762	
-5.03591	10.60182	
-4.75993	10.64551	
-4.48394	10.68831	
-4.20795	10.72984	
-3.93196	10.76974	
-3.65597	10.80765	
-3.37998	10.84323	
-3.10398	10.87617	
-2.82799	10.90619	
-2.55199	10.93300	
-2.27600	10.95639	
-2.00000	10.97614	
-1.80643	10.98673	
-1.61266	10.99320	
-1.45879	10.99591	
-1.27962	11.00000	FAN LE
-1.14030	11.01530	
-1.00090	11.02880	
-0.86160	11.04060	
-0.72220	11.05060	
-0.58290	11.05880	
-0.44360	11.06530	
-0.30420	11.07000	
-0.16490	11.07290	
-0.02550	11.07410	
0.11380	11.07360	
0.25310	11.07130	
0.39250	11.06720	
0.53180	11.06140	
0.67120	11.05380	
0.81050	11.04450	
0.94980	11.03340	
1.08920	11.02050	
1.22850	11.00580	
1.36790	10.98940	
1.50721	10.97110	FAN TE
1.65878	10.97216	
1.83588	10.97521	
2.01306	10.98232	
2.19020	10.99080	
2.36724	10.99985	
2.54408	11.00980	
2.72078	11.02104	
2.89729	11.03393	
3.07360	11.04885	
3.24967	11.06616	
3.42549	11.08597	
3.60114	11.10800	
3.77658	11.13193	
3.95188	11.15744	
4.12702	11.18421	
4.30205	11.21193	
4.47701	11.24017	
4.65198	11.26818	
4.82704	11.29513	
5.00231	11.32018	
5.17787	11.34253	
5.35382	11.36133	
5.53021	11.37609	
5.70693	11.38736	
5.88387	11.39589	
6.06088	11.40241	
6.23792	11.40719	
6.41496	11.40986	
6.59200	11.41000	FEGV LE
6.77390	11.40718	
6.95575	11.40141	
7.13751	11.39281	
7.31915	11.38153	
7.50061	11.36751	
7.68184	11.35073	
7.86302	11.33369	
8.04434	11.31918	
8.22600	11.31000	FEGV TE
8.38965	11.30471	
8.55326	11.29925	
8.71688	11.29415	
8.88057	11.28994	
9.04498	11.28770	
9.21092	11.28798	
9.37866	11.29056	
9.54846	11.29525	
9.72058	11.30185	
9.89530	11.31015	
10.07286	11.31996	
10.25357	11.33105	
10.43769	11.34325	
10.62544	11.35633	
10.81713	11.37011	
11.01302	11.38437	
11.21337	11.39891	
11.41844	11.41354	
11.62853	11.42805	
11.84387	11.44223	
12.06474	11.45588	
12.29143	11.46881	
12.52417	11.48080	
12.76325	11.49166	
13.00893	11.50119	
13.26148	11.50917	
13.52117	11.51541	
13.78824	11.51970	
14.06299	11.52184	
14.34567	11.52164	
14.63657	11.51888	
14.93595	11.51337	
15.24404	11.50489	
15.56114	11.49326	
15.88751	11.47826	
16.22343	11.45969	
16.56917	11.43736	
16.92496	11.41105	
17.29109	11.38056	
17.66785	11.34570	
18.05547	11.30626	
18.45422	11.26204	
18.86441	11.21283	
19.28625	11.15843	
19.72005	11.09865	
20.16605	11.03326	
20.62453	10.96209	
21.09576	10.88491	
21.58000	10.80153	

Table B-2. Fan Inner Flowpath

AXIAL	RADIUS	AXIAL	RADIUS		AXIAL	RADIUS	
-7.74119	0.0	-4.93973	3.69333		1.47104	4.98254	
-7.74023	0.07657	-4.85016	3.73771		1.59011	4.98632	
-7.73735	0.15289	-4.75947	3.78123		1.70911	4.98924	
-7.73258	0.22894	-4.66766	3.82387		1.82797	4.99064	
-7.72591	0.30471	-4.57475	3.86563		1.94661	4.98985	
-7.71738	0.38019	-4.48076	3.90649		2.06496	4.98620	
-7.70698	0.45537	-4.38569	3.94645		2.18295	4.97901	
-7.69473	0.53025	-4.28956	3.98550		2.30049	4.96766	
-7.68066	0.60480	-4.19239	4.02361		2.41760	4.95216	
-7.66476	0.67902	-4.09418	4.06080		2.80000	4.86000	
-7.64706	0.75290	-3.99496	4.09703		3.24000	4.73000	
-7.62757	0.82642	-3.89473	4.13232		3.50000	4.64000	
-7.60630	0.89959	-3.79350	4.16663		3.89000	4.51500	S1 LE
-7.58326	0.97238	-3.69130	4.19996		4.24200	4.43000	
-7.55847	1.04479	-3.58813	4.23231		4.67300	4.38700	S1 TE
-7.53194	1.11681	-3.48402	4.26366		5.17000	4.40000	
-7.50369	1.18842	-3.37896	4.29400		5.91000	4.47500	
-7.47373	1.25962	-3.27298	4.32332		6.74000	4.57500	
-7.44207	1.33040	-3.16609	4.35161		7.80000	4.70000	
-7.40873	1.40073	-3.05831	4.37886		10.1000	4.70000	
-7.37372	1.47063	-2.94964	4.40506		12.2100	4.70000	
-7.33705	1.54006	-2.84010	4.43020		27.6300	4.70000	
-7.29874	1.60904	-2.72970	4.45427		34.0000	4.70000	
-7.25880	1.67753	-2.61846	4.47725				
-7.21724	1.74554	-2.50639	4.49914				
-7.17408	1.81304	-2.39351	4.51993				
-7.12933	1.88005	-2.27982	4.53961				
-7.08301	1.94653	-2.16535	4.55816				
-7.03513	2.01248	-2.05010	4.57558				
-6.98569	2.07789	-1.93409	4.59186				
-6.93473	2.14276	-1.81733	4.60697				
-6.88224	2.20706	-1.69988	4.62100				
-6.82824	2.27079	-1.58227	4.63476				
-6.77275	2.33395	-1.46466	4.64853				
-6.71578	2.39651	-1.34705	4.66230				
-6.65735	2.45846	-1.22944	4.67607				
-6.59746	2.51981	-1.08416	4.69000	FAN LE			
-6.53613	2.58053	-0.99463	4.69671				
-6.47338	2.64062	-0.87629	4.70176				
-6.40921	2.70007	-0.75779	4.70533				
-6.34364	2.75886	-0.63910	4.70777				
-6.27669	2.81698	-0.52019	4.70943				
-6.20837	2.87443	-0.40116	4.71115				
-6.13869	2.93120	-0.28229	4.71462				
-6.06767	2.98727	-0.16388	4.72159				
-5.99531	3.04263	-0.04626	4.73382				
-5.92164	3.09728	0.07029	4.75292				
-5.84666	3.15120	0.18586	4.77832				
-5.77039	3.20438	0.30081	4.80779				
-5.69285	3.25682	0.41551	4.83904				
-5.61404	3.30849	0.53034	4.86978				
-5.53398	3.35940	0.64565	4.89775				
-5.45269	3.40952	0.76177	4.92095				
-5.37017	3.45886	0.87871	4.93930				
-5.28645	3.50740	0.99634	4.95348				
-5.20153	3.55512	1.11450	4.96420				
-5.11542	3.60203	1.23311	4.97215				
-5.02815	3.64810	1.35640	4.97803	FAN TE			

Table B-3. Fan Duct Inner Flowpath

AXIAL	RADIUS		AXIAL	RADIUS	AXIAL	RADIUS
3.74000	5.55000		15.52074	6.95323	31.15733	4.66212
3.75000	5.58100		15.79044	6.98597	31.42587	4.59516
3.76000	5.59450		16.06020	7.01760	31.69441	4.52821
3.78000	5.61600		16.33003	7.04788	31.96295	4.46125
3.83000	5.65400		16.59995	7.07658	32.23149	4.39430
3.90000	5.68850		16.86996	7.10349	32.50003	4.32734
4.00000	5.72600		17.14008	7.12836	32.76859	4.26039
4.10000	5.75300		17.41032	7.15097	33.03712	4.19343
4.20000	5.77450		17.68071	7.17109	33.30566	4.12648
4.30000	5.79100		17.95123	7.18849	33.57420	4.05952
5.25000	5.81000		18.22192	7.20294	33.84274	3.99257
5.60000	5.81000		18.49278	7.21421	34.11128	3.92561
5.99000	5.81000		18.76382	7.22207	34.37982	3.85866
6.30000	5.81000		19.03506	7.22629	34.64836	3.79170
6.59200	5.81000	FEGV LE	19.30650	7.22664	34.91690	3.72475
6.77400	5.82900		19.57817	7.22289		
6.97400	5.87900		19.85008	7.21481		
7.17400	5.95200		20.12224	7.20218		
7.37400	6.03900		20.39465	7.18476		
7.57400	6.12700		20.66734	7.16232		
7.77400	6.21000		20.94031	7.13463		
7.97400	6.28200		21.21358	7.10147		
8.22600	6.35000	FEGV TE	21.48712	7.06231		
8.37400	6.37600		21.75836	7.00554		
8.57400	6.39900		22.02692	6.93859		
8.77400	6.41400		22.29546	6.87163		
8.97400	6.42600		22.56400	6.80468		
9.17400	6.43900		22.83253	6.73772		
9.37400	6.45100		23.10107	6.67077		
9.57400	6.46400		23.36961	6.60381		
9.77400	6.47500		23.63815	6.53686		
9.97400	6.48600		23.90671	6.46990		
10.17400	6.49500		24.17525	6.40295		
10.37400	6.50400		24.44379	6.33599		
10.57400	6.51200		24.71233	6.26904		
10.77400	6.52000		24.98087	6.20208		
11.97400	6.52800		25.24940	6.13513		
11.17400	6.53700		25.51796	6.06817		
11.37400	6.54500		25.78650	6.00122		
11.57400	6.55500		26.05504	5.93426		
11.77400	6.56600		26.32358	5.86731		
11.97400	6.57800		26.59212	5.80035		
12.17400	6.59100		26.86066	5.73340		
12.37400	6.60600		27.12921	5.66644		
12.57400	6.62300		27.39775	5.59949		
12.77400	6.64000		27.66629	5.53253		
12.97400	6.65900		27.93483	5.46558		
13.17400	6.67900		28.20337	5.39862		
13.37400	6.69900		28.47191	5.33167		
13.57400	6.72100		28.74046	5.26471		
13.77400	6.74300		29.00900	5.19776		
13.97400	6.76600		29.27754	5.13080		
14.17400	6.79000		29.54608	5.06385		
14.37400	6.81400		29.81462	4.99689		
14.57400	6.83800		30.08316	4.92994		
14.71187	6.85064		30.35170	4.86298		
14.98146	6.88534		30.62025	4.79603		
15.25109	6.91961		30.88879	4.72907		

Table B-4. Core Outer Flowpath

AXIAL	RADIUS	
3.74000	5.55000	
3.75000	5.49900	
3.76000	5.48300	
3.78000	5.46000	
3.83000	5.42200	
3.90000	5.38450	
4.00000	5.34550	
4.12000	5.31000	S1 LE
4.51300	5.24200	
4.90300	5.20200	S1 TE
5.41000	5.20500	
5.91000	5.27500	
6.74000	5.36400	
7.80000	5.41000	
10.1000	5.41000	
12.2100	5.41000	
27.6300	5.41000	
34.0000	5.96750	

APPENDIX C — HARDWARE SAFETY MARGINS

Feature	Maximum Principal Stress (ksi)	Yield Margin of Safety	Ultimate Margin of Safety	Life (cycles)
Blade Airfoil	52.7	0.7	1.0	Stage Life > 1,000
Blade Attachment	20.5	1.1	1.4	Stage Life > 1,000
Spinner	21.9	5.3	5.8	Life >1,000
Torque Sleeve	22.0	5.3	5.8	Life >1,000
Pitch Plug	17.0	7.2	7.8	Life >1,000
Disk	78.6	0.7	0.9	Life >1,000
Seal	10.6	12.0	13.1	Life >1,000
Balance Ring	25.2	4.5	4.9	Life >1,000
FEGV	157.0	-	-0.05	Life >1,000

REPORT DOCUMENTATION PAGE

Form Approved
OMB No. 0704-0188

1. AGENCY USE ONLY (*Leave blank*)	2. REPORT DATE	3. REPORT TYPE AND DATES COVERED
	December 1997	Final Contractor Report

4. TITLE AND SUBTITLE

Advanced Low-Noise Research Fan Stage Design

5. FUNDING NUMBERS

WU–538–03–12–00
NAS3–26618

6. AUTHOR(S)

Robert Neubert, Larry Bock, Eric Malmborg, and William Owen-Peer

7. PERFORMING ORGANIZATION NAME(S) AND ADDRESS(ES)

United Technologies Corporation
Pratt & Whitney
East Hartford, Connecticut 06108

8. PERFORMING ORGANIZATION REPORT NUMBER

E–11006

9. SPONSORING/MONITORING AGENCY NAME(S) AND ADDRESS(ES)

National Aeronautics and Space Administration
Lewis Research Center
Cleveland, Ohio 44135–3191

10. SPONSORING/MONITORING AGENCY REPORT NUMBER

NASA CR—97-206308

11. SUPPLEMENTARY NOTES

Project Manager, Brian Fite, Structures and Acoustics Division, NASA Lewis Research Center, organization code 5940, (216) 433–3892.

12a. DISTRIBUTION/AVAILABILITY STATEMENT

Unclassified - Unlimited
Subject Category: 07 Distribution: Nonstandard

This publication is available from the NASA Center for AeroSpace Information, (301) 621–0390.

12b. DISTRIBUTION CODE

13. ABSTRACT ***(Maximum 200 words)***

This report describes the design of the Advanced Low-Noise Research Fan stage. The fan is a variable pitch design, which is designed at the cruise pitch condition. Relative to the cruise setting, the blade is closed at takeoff and opened for reverse thrust operation. The fan stage is a split flow design with fan exit guide vanes (FEGVs) and core stators. The fan stage design is combined with a nacelle and engine core duct to form a powered fan/nacelle subscale model. This model is intended for use in combined aerodynamic, acoustic, and structural testing in a wind tunnel. The fan has an outer diameter of 22 in. and a hub-to-tip of 0.426 in., which allows the use of existing NASA fan and cowl force balance and rig drive systems. The design parameters were selected to permit valid acoustic and aerodynamic comparisons with the Pratt & Whitney (P&W) 17- and 22-in. rigs previously tested under NASA contract. The fan stage design is described in detail. The results of the design axisymmetric and Navier-Stokes aerodynamic analysis are presented at the critical design conditions. The structural analysis of the fan rotor and attachment is included. The blade and attachment are predicted to have adequate low-cycle fatigue life and an acceptable operating range without resonant stress or flutter. The stage was acoustically designed with airfoil counts in the FEGV and core stator to minimize noise. A fan/ FEGV tone analysis developed separately under NASA contract was used to determine the optimum airfoil counts. The fan stage was matched to the existing nacelle, designed under the previous P&W low-noise contract, to form a fan/nacelle model for wind tunnel testing. It is an axisymmetric nacelle for convenience in testing and analysis. Previous testing confirmed that the nacelle performed as required at various aircraft operating conditions.

14. SUBJECT TERMS	15. NUMBER OF PAGES
Turbofan; Low noise; Variable pitch; Low pressure ratio; Ducted fan	71
	16. PRICE CODE A04

17. SECURITY CLASSIFICATION OF REPORT	18. SECURITY CLASSIFICATION OF THIS PAGE	19. SECURITY CLASSIFICATION OF ABSTRACT	20. LIMITATION OF ABSTRACT
Unclassified	Unclassified	Unclassified	